Parametric Study of seismic vehicular damping using structural hysteresis and viscoelastic material

By

NS Muhammad Saad Ali

00000204464

MS-17

Submitted to the Department of Mechanical Engineering in Fulfillment of the

Requirements for the Degree of

MASTER OF SCIENCE

In

MECHANICAL ENGINEERING

Thesis Supervisor

Hasan Aftab Saeed, PhD

College of Electrical & Mechanical Engineering

National University of Sciences & Technology

2019

Parametric Study of seismic vehicular damping using structural hysteresis and viscoelastic material

Author

Muhammad Saad Ali

00000204464

A thesis submitted in partial fulfillment of the requirements for the degree of

MS Mechanical Engineering

Thesis Supervisor:

Dr. Hasan Aftab Saeed

Thesis Supervisor's Signature: _____

DEPARTMENT OF MECHANICAL ENGINEERING

COLLEGE OF ELECTRICAL & MECHANICAL ENGINEERING

NATIONAL UNIVERSITY OF SCIENCES AND TECHNOLOGY,

ISLAMABAD

August , 2019

بِسْمِ اللهِ الرَّحْمٰنِ الرَّحِيْمِ

In the name of Allah, the most Beneficent and the most Merciful

Declaration

I hereby affirm that this thesis Title "**Parametric study of seismic vehicular damping using structural hysteresis and viscoelastic material"** is absolutely based upon my own personal hard work under the valuable guidance of my supervisor Dr Hasan Aftab Saeed. The Contents have not been plagiarized and sources used are cited. No part of work presented in thesis has been submitted in favor of any application of other degree of qualification to this or any other university or institute of learning.

………………………

Muhammad Saad Ali

LANGUAGE CORRECTNESS CERTIFICATE

This thesis has been read by an English expert and is free of typing, syntax, semantic, grammatical and spelling mistakes. Thesis is also according to the format given by the university.

<div align="right">

_____

Signature of Student
NS Muhammad Saad Ali
00000204464

_____

Signature of Supervisor
(Dr Hasan Aftab Saeed)

</div>

PLAGIARISM CERTIFICATE (TURNITIN REPORT)

This thesis has been checked by plagiarism in turnitin. The report countersigned by respective supervisor is attached along with.

<div align="right">

Signature of student

Muhammad Saad Ali

00000204464

</div>

<div align="right">

Signature of supervisor

Dr Hasan Aftab Saeed

</div>

Copyright Statement

ACKNOWLEDGEMENTS

First and foremost, I would like to thank my Almighty Allah for all His countless blessings and benevolence which embraced me to complete this incredible task in terms of integrity and completeness.

Secondly, there is long list of people without whom I would have not been able to complete this assignment successfully. I would like to communicate special recognition and gratitude to my advisor,

Dr. Hasan Aftab Saeed for his extended support throughout my thesis tenure. His untiring efforts and advice helped me to move around every predicament during my research work.

 I would also like to thank Assistant Professor **Dr. Sajidullah Butt** and special thanks to **Dr Naveed Akmal Din**, for serving as my Guidance and Evaluation committee even at hardship. I obliged for letting my defense as enjoyable moments and for brilliant comments and suggestions.

Special thanks to my **family**; **my mother**, **father** and siblings for all the sacrifices that they made and who were always in my support in dire moments. Conclusively, I would like to thank the entire honorable faculty of Department of Mechanical Engineering, whose professional approach and vision groomed me as a sound person both technically and morally.

Muhammad Saad Ali, 2017

DEDICATIONS

➢ I dedicate my thesis to my family and friends. A special feeling of gratitude to my loving parents, whose words of encouragement were always there in my moral support.

➢ I would place sincere thanks to Dr. Hasan Aftab Saeed for his guidance and support throughout this study, and specially his confidence in me.

➢ I pray ALLAH, for always being kind by way His countless blessings.

Abstract

In design of damper energy dissipation in a very deterministic and sophisticated manner is needed the isolation systems usually made of viscoelastic material damps only the modal natural frequencies of seismic-vehicular vibrations and larger deformation but inadequate structural hysteresis. In MR damper fluid leakage is the key issue, requires electric supply as well as costlier sensor which on seismic fragility gets damaged, so they are less reliable but active dampers modifies themselves according to state of structure using electronic acquisition and feedback control systems, but these are affected by catastrophe. So, moving towards passive damping includes displacement-activated metallic, friction and viscoelastic Dampers, motion activated tuned dampers (TMD, TLD) while velocity activated viscous dampers. Passive dampers are reliable during havoc but unable to modify according to need they are velocity, displacement dependent.

Presenting seismic-vehicular damping making dampers independent of velocity and increasing sensitivity of metallic damper as well as stiffness using displacement-controlled loading and activation sensitive yield points using different boundary conditions with modified steel rods for applying loading to enhance structural hysteresis and by introducing the lamination of viscoelastic materials we will be independent of velocity-controlled boundary conditions by performing material damping using polyurethane to damp resonance of first modes of vibrations lying at frequencies in the order of thousands which are very higher than the dynamic response of bridge vehicle interaction by introducing thin laminates of viscoelastic polyurethane. Parametric study not only reveals the sensitivity of plastic deformation but also interrelated to dimensions of the U-shaped structural steel also by reducing the cyclic numerical error using combined hardening parameters.

Table of Contents

LIST OF FIGURES

LIST OF TABLES

CHAPTER 1

INTRODUCTION

Reduction in the amplitude of oscillation by draining energy out of the system and may be utilized or simply dissipated as in structural hysteresis. By damping the different modes of vibration, we can also achieve that like in material and structural damping. Structural damping is facilitated by applying specified materials such as polyurethane to enhance material damping as a viscoelastic material has good damping abilities. Structural as well as the material damping ratio as very high for constructional and structural steel and therefore a composite must be developed to be used as multipurpose. There are different sources of vibration they may be seismic, tidal, wind-based, vehicular, rotating and static machine. These all are concerned with fragilities.

Dampers are therefore a solution towards these problems which are installed usually between bridge pier and girder in order to respond against different seismic intensities like hysteretic steel damper, Liquid Tuned dampers (LTD), Mass Tuned Dampers (MTD). Seismic drift demands and need of isolation systems for prevention of havoc. (FRF) frequency response functions, hysteresis loops, fatigue life, stiffness and active yield points generated by simulating the results. Cost-effectiveness of passive damping devices rather than to use active devices by modifying according stimulus. Introducing new assemblies with varying boundary conditions in order to increase the sensitivity towards plastic deformation and trying different thickness of polyurethane laminate.

1.1   Aim and Goal

Improvement in hysteresis energy by using different geometries assembled with different load transmission member combining with different viscoelastic and steel material in order to make damper dual purpose, passive but very sensitive hence cost effective. Eliminating the problem of fluid leakage as in magnetorheological damper (MR) damper and liquid tuned damper (LTD).

Enhancing deformation and energy dissipation capacity using strain-controlled loading to reduce the need for sensors in passive damping devices. Facilitation of material damping with hysteretic damping is a big step forward.

1.2 Damping and its types

Damping is categorized into three universal categories which are active, semi-active and passive damping devices almost all the dampers are the daughter. Active damping devices requires sensors with an electric power supply to impart stimulus and get feedback in accordance to which a damper is modified with respect to nature and intensity of shock like in MR dampers.

while in semi-active damping devices like in liquid tuned damping and MTD requires some abilities adopting response by columnar level of liquid and variation in mass and some aspects are covered with control mechanisms with a very little power supplied only to run sensors, so they are semi-modified.

As far as the passive damping devices are concerned there is no need of sensors hence increased reliability as they are very less exposed to damage due to different seismic intensities and other vibrations. They are unable to treat variable, different nature and different sources of vibrations.

1.3 Key Issues and advantages of different damping

1.3.1   Active damper are very exposed to damage because they have sensors which are sensitive especially during high seismic intensities. They are costliest. They Need power supply so they will not work when the power is shutdown.

1.3.2   Passive damping devices are more reliable less costlier than active and semi-active damping devices. No need of power supplied and very less exposed to damage but they are not adoptable in response to variation

1.3.3   Semi-active damping device need feedback control systems with little power supplied for working but like active devices they are greatly exposed to damage and costlier. Higher manufacturing cost because of sensors installed.

1.3.4   Different subtypes of dampers are then made like viscous dampers, mass tuned, liquid tuned dampers, MR dampers having different issues like fluid leakage. Shear Panels have low stiffness and deformation capacity to dissipate shocks.

1.3.5   Ideal geometries and assemblies are required to work damper effectively. The

geometries are such that they are simple to install between bridge pier and girder as fig 1,2
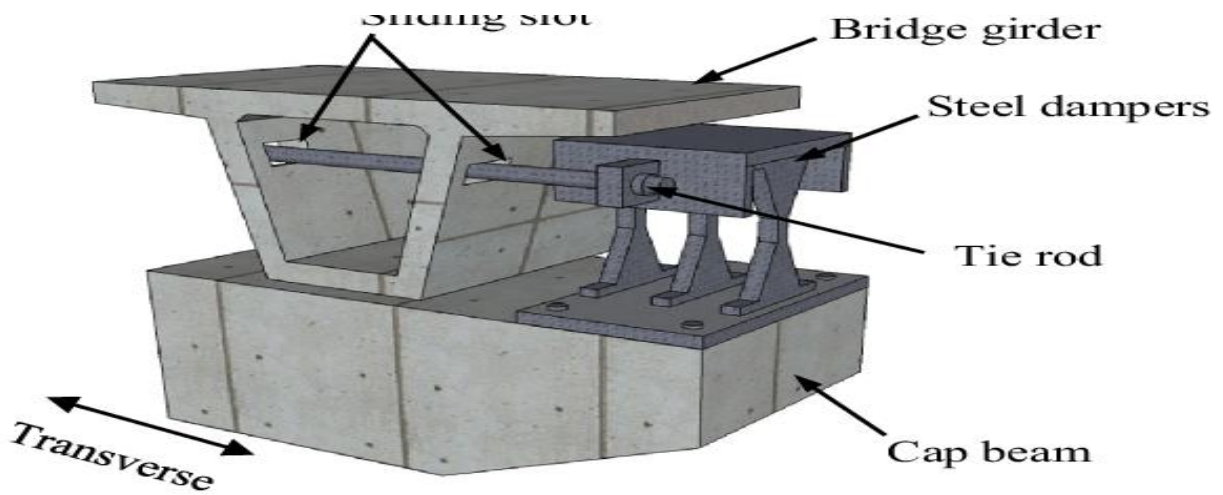
Figure 1: Bridge Pier
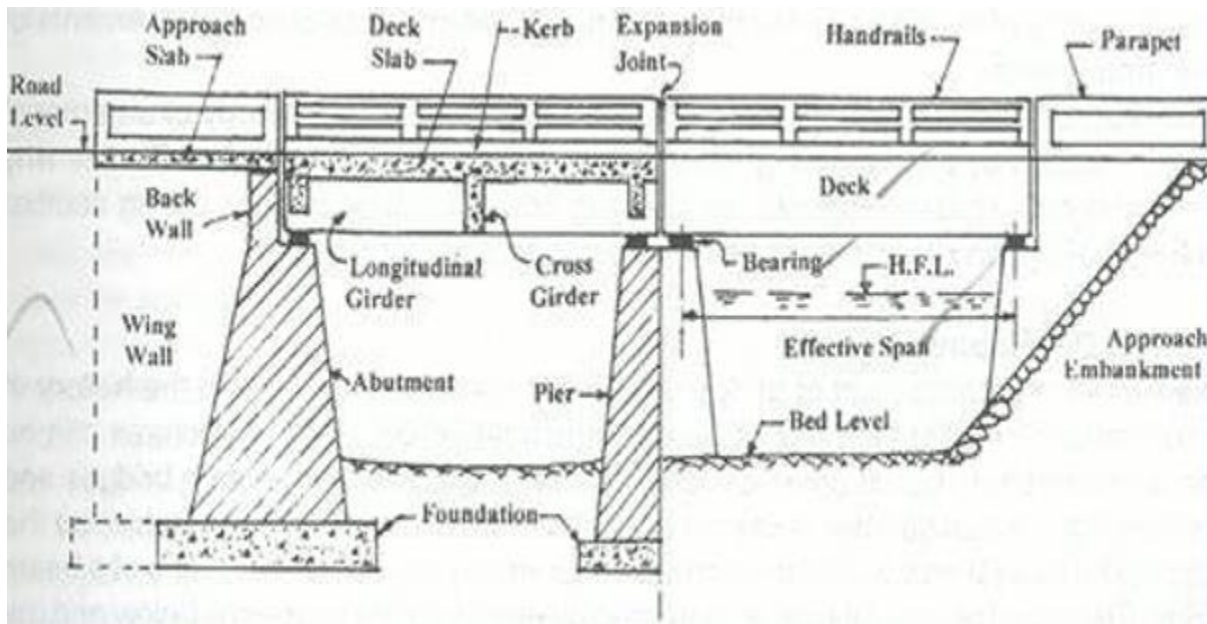
Figure 2: Bridge Girder and Pier

1.4 OUTLINE OF THE PROPOSED SYSTEM

Our aim is to create achieve the goal given in the figure below by using different parameters like thickness, radius, height, length etc. of the damper
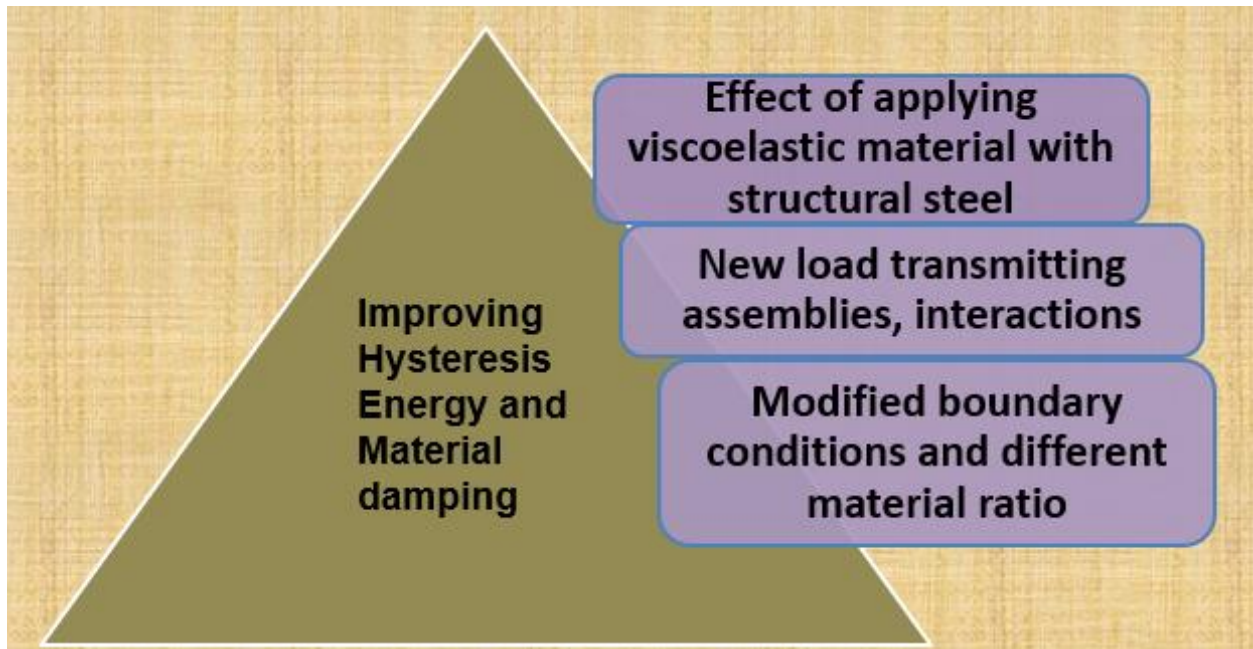
1.5 STRUCTURE OF THE THESIS

There are six chapters in the current thesis. The introductory section begins with a debate on damping and its types, key issues, sources of vibrations, geometries dependency on dampers.

Chapter 2 Current chapter is an analysis of the journal papers on the structural hysteresis, material damping, cyclic responses, low cycle fatigue, combined hardening model, crystal plasticity, shear-bending combined damping, types of damper, sources of vibrations, types of structures like buildings, bridges requiring damping and sources of vibrations like seismic-vehicular requires different types of dampers and damping.

Chapter 3 Presents the methodology used for creating 3D CAD model in Abaqus or in CRE-O then step file is imported. After importing model properties are assigned like elasticity, plasticity, loss modulus etc. to specify material. Then in the interaction module different geometries are coupled and then assembled in assembly module. After this step module uses static general or SSD. After this module mesh is generated in mesh module using C3D8R/H and C3D20R/H. Nodal responses are then extracted from the simulation results inform of FRF and hysteresis loop.

Chapter 4 Presents previous and current researches regarding damping structures and dynamic response of a vehicle on bridge where vehicle at different velocities behaves as a vibration shaker. Calculating resonant frequencies for given bridge parameters and

boundary conditions for specific velocity of vehicle at different positions

Chapter 5 Presents parametrize results for energy dissipation and damping ability in a single type explaining (FRF) variant hysteresis loop response. Optimization purpose and some analysis like low cycle fatigue are required that will lead to design and are ready for discussion.

Chapter 6 Explains the end results/conclusions and scope of current work in future. From the results discussed in chap5 we can easily conclude some facts that how different parameters affects the energy dissipation capability. What are the steps taken by the manufacturer to implement it in real practice?

CH#1	Introduction
CH#2	Literature Review
CH#3	Detailed methodology adopted for Abaqus simulation. Extraction of results from FRF and hysteresis loops. Damping calculated using half power point method in MATLAB
CH#4	Case Study
CH#5	Results and discussions
CH#6	Conclusion and future perspective
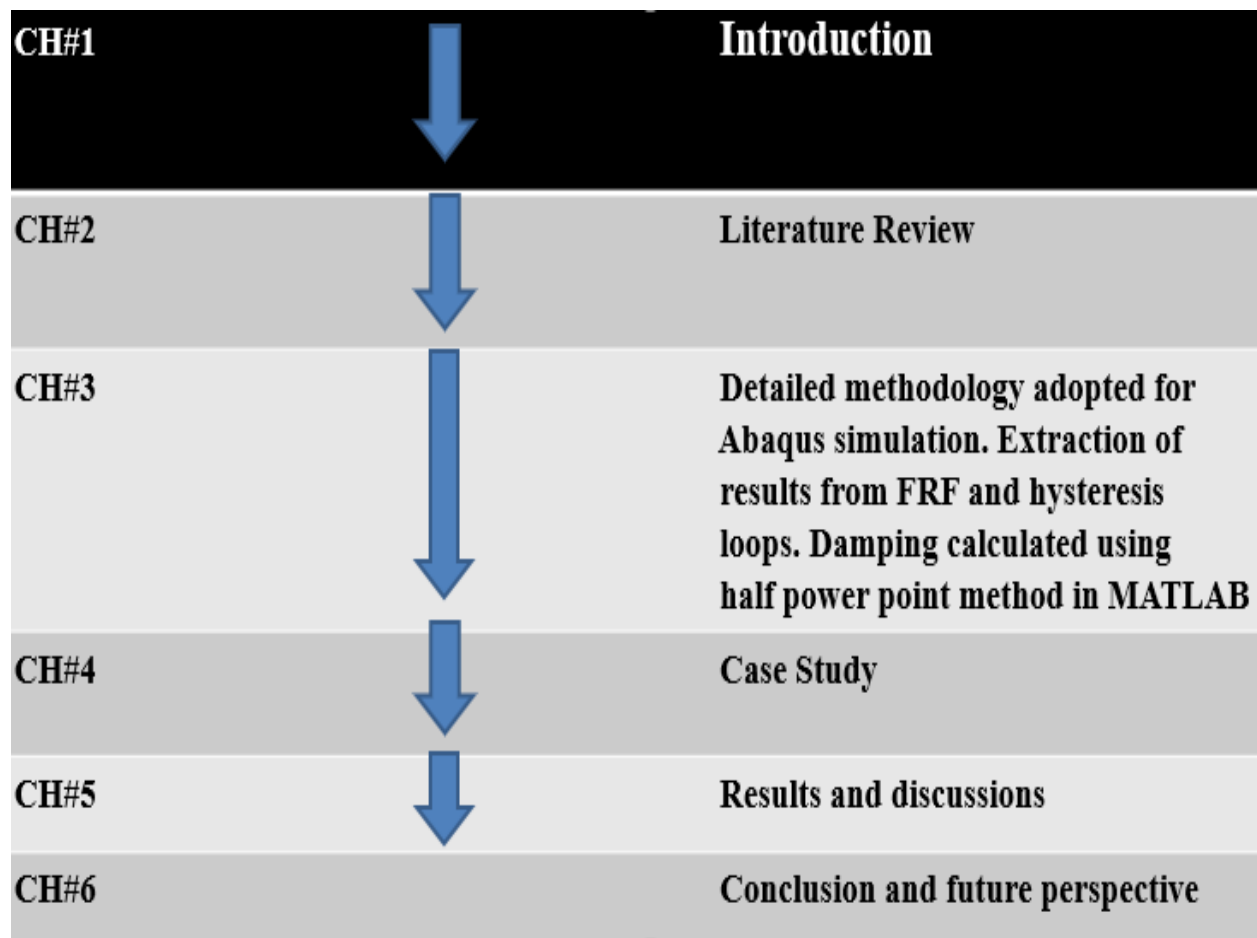
Figure 3: Structure of Thesis

Deposition of Thesis Report
At the end of the dissertation, a list of references is added

CHAPTER 2

LITERATURE REVIEW

In this chapter a base is formed in a sophisticated way that reader can easily understand the research related to damping and its configuration. Different types of dampers used by previous researchers with different dissipations capacities. Major types like ADAS, TADAS, CAR, PMD, C.D, viscous, friction, hysteretic, LTD, MTD, S.P. Interaction with different vehicle-bridge parameters and different sources of vibrations like seismic intensities etc.

2.1 Dynamic response of vehicle on bridge

The paper worked on developed the mathematical model which calculated the first modal frequencies of vehicle passing over the bridge. The equipment installed for doing so is very expensive, difficult to use and place. In this paper the passed vehicle behaved as a vibration shaker and the bridge is a simply supported beam which responds at different frequencies corresponding to velocity of passed vehicle. A condition came depending upon the velocity of vehicle where the first modal frequency of the bridge and vehicle is very close hence resonance occurred. The frequency measured was high midway of bridge while low at the end of the bridge. The bridge with large stiffness had high modal frequency and this was well for bridge in order to avoid resonance. In order to measure the stiffness or strength degradation of the bridge by overloading or seismic fragility frequencies of newly prepared bridge and the same bridge after some period of consumption is measured hence compared. Vehicle-bridge interaction is developed, and analytical formulation was made which was also compared with FEM model.

2.1.a Mathematical Model

This work assumed if vehicle was moving with velocity v having mass m_v and stiffness k and behaves as a sprung mass. The length of the bridge was L and damping is ignored then equation of motion for vehicle and bridge are as

$$m_v \ddot{q}_v + k_v(q_v - u|_{x=vt}) = 0 \tag{1}$$

$$m\ddot{u} + EIu'''' = f_c(t)\delta(x - vt) \tag{2}$$

q is the vertical deflection of the sprung mass, m_v is sprung mass and m is the mass of bridge per unit length. E is elastic modulus and I is the moment of inertia. The contact force between sprung mass and beam is given by

$$f_c(t) = k_v(q_v - u|_{x=vt}) + m_v g \tag{3}$$
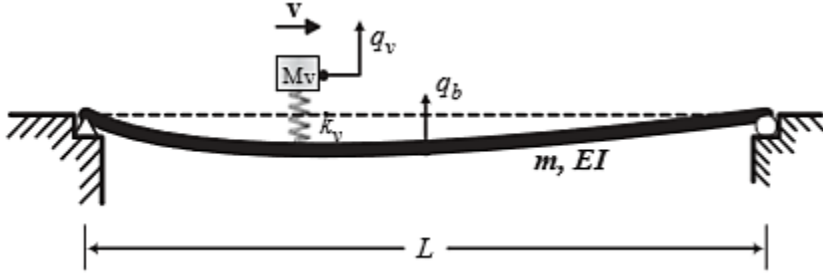
g is the acceleration due to gravity The response of beam for moving transient load is

$$u(x, t) = q_b(t) \, \sin\left(\frac{\pi x}{L}\right) \tag{4}$$

Substituting the value of beam displacement from equation 4 in equation 1 and 2
We get

$$m_v \ddot{q}_v + (\omega_v^2 m_v)q_v - \left[\omega_v^2 m_v \sin\left(\frac{\pi v t}{L}\right)\right]q_b = 0 \tag{5}$$

$$\frac{mL}{2}\ddot{q}_b + \left[\frac{mL}{2}\omega_b^2 + \omega_v^2 m_v \sin^2\left(\frac{\pi v t}{L}\right)\right]q_b - \left[\omega_v^2 m_v \sin\left(\frac{\pi v t}{L}\right)\right]q_v = -m_v g \sin\left(\frac{\pi v t}{L}\right) \tag{6}$$

$$\omega_v = \sqrt{\frac{k_v}{m_v}}, \quad \omega_b = \frac{\pi^2}{L^2}\sqrt{\frac{EI}{m}} \tag{7}$$

Where ω_v and ω_b denote the vibration frequency of the vehicle and the bridge, respectively. The solution is closed form and we need real practice. Now consider a simulation by finite element model the equation then generated only for a single element is given as

$$\begin{bmatrix} m_v & 0 \\ 0 & [m_b] \end{bmatrix} \begin{Bmatrix} \ddot{q}_v \\ \{\ddot{u}_b\} \end{Bmatrix} + \begin{bmatrix} c_v & -c_v\{N\}^{\mathrm{T}} \\ -c_v\{N\} & [c_b] + 2vm_v\{N\}\dfrac{\partial\{N\}^{\mathrm{T}}}{\partial x} + c_v\{N\}\{N\}^{\mathrm{T}} \end{bmatrix} \begin{Bmatrix} \dot{q}_v \\ \{\dot{u}_b\} \end{Bmatrix}$$

$$+ \begin{bmatrix} k_v & -k_v\{N\}^{\mathrm{T}} \\ -k_v\{N\} & [k_b] + v^2 m_v\{N\}\dfrac{\partial^2\{N\}^{\mathrm{T}}}{\partial x^2} + vc_v\{N\}\dfrac{\partial\{N\}^{\mathrm{T}}}{\partial x} + k_v\{N\}\{N\}^{\mathrm{T}} \end{bmatrix} \begin{Bmatrix} q_v \\ \{u_b\} \end{Bmatrix} = \begin{Bmatrix} 0 \\ -m_v g\{N\}_c \end{Bmatrix}. \quad (8)$$

$$[M]\{\ddot{q}\} + [C]\{\dot{q}\} + [K]\{q\} = \{F\} \quad (9)$$

Where c_b is damping k_b are stiffness matrices of bridge. After finding the solution the results are compared with analytical model and ready to use

2.1.b   Resonant Case

Condition of resonance for the parameters of bridge given below

L	25m
E	27.5GPa
M/L	4800 Kg/m
m	1200kg
k	296KN/m
I	$0.12m^4$
A	$2m^2$

Table 1: Parameters of bridge and vehicle

Because the fundamental frequency of the bridge contained in the vehicle response shifts as the vehicle speed v increases, there is a possibility for the occurrence of resonance if the shifted frequency$\omega_b + \frac{\pi v}{L}$ becomes equal or close to the vehicle frequency. which implies a vehicle frequency of ω_v =2.50 Hz. If the vehicle speed is selected as 20m/s(=72km/h), then the shifted frequency $\omega_b + \frac{\pi v}{L}$ is 2.48Hz, which is quite close to the vehicle frequency ω_v. FRF calculated for both bridge and vehicle are shown below in Fig 4 with damping, Fig

5 with high stiffness bridge and Fig 6 with resonance
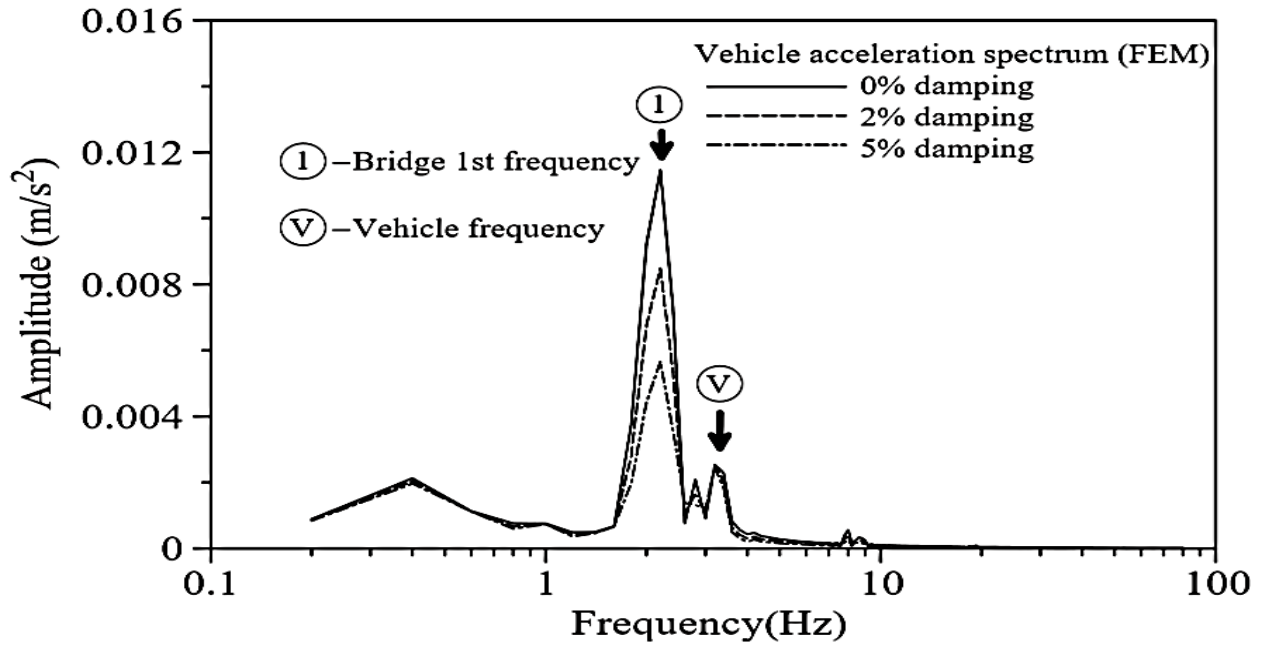
Figure 4: Acceleration Spectrum of low stiffness bridge
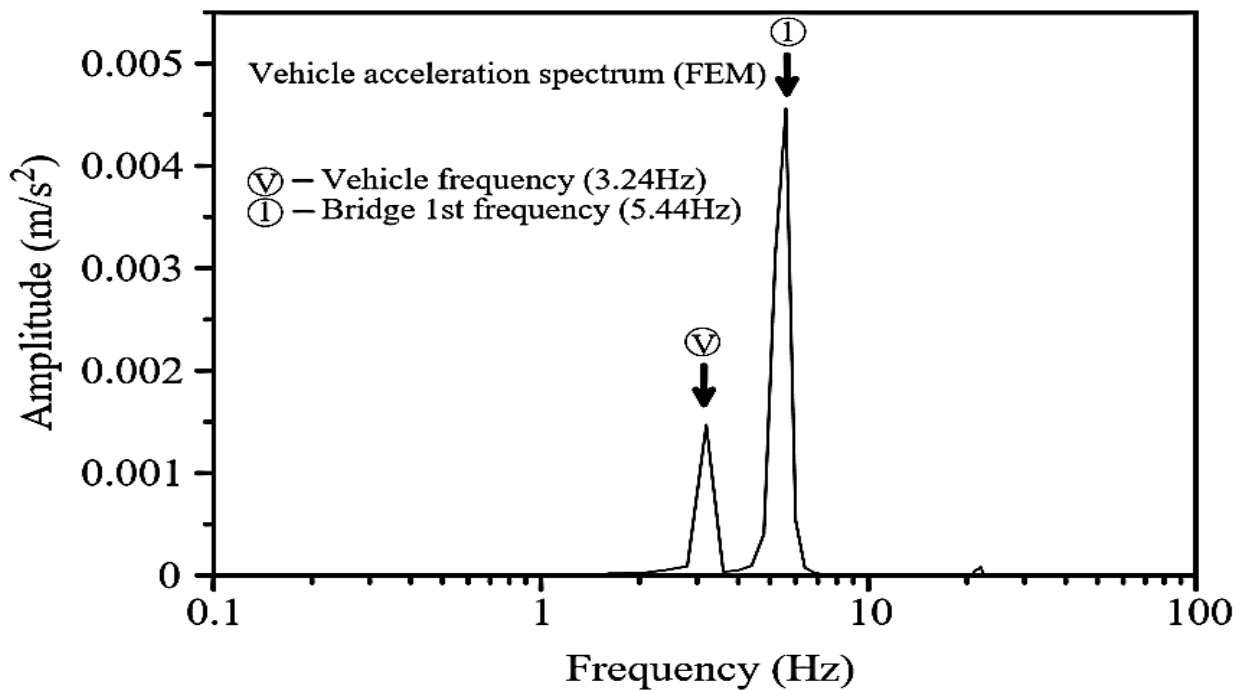
Figure 5: Acceleration spectrum of High stiffness Bridge
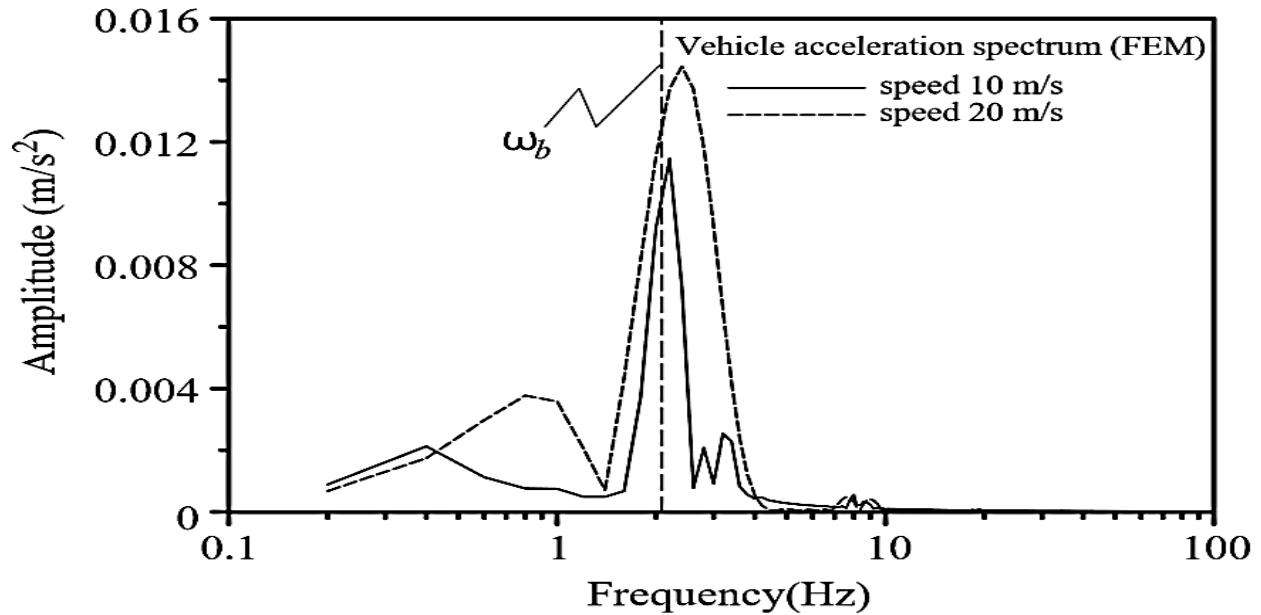
Figure 6: Acceleration spectrum of bridge-vehicle resonance case

2.2 Crawler steel damper

A U-shaped dissipation plate is presented in this research with a new assembly to enhance yielding with better low cycle fatigue hence fulfilling requirements of deformation and strength. Cyclic responses with low cycle fatigue analysis are controlled by varying the parameters of dampers which include thickness, height of dissipation plates by including and excluding connection plates. Equations of compatibility and equilibrium were derived. Finite element analysis was performed in Abaqus to supplement physical test results by applying cyclic loading schemes. Hysteresis loops a formed are stabilized and saturated. Combined hardening model was used to reduce numerical error. Isolation systems were used to protect bridge from seismic vibrations by protecting pier and girder. They survive very large displacement but small stiffness hence inadequate energy dissipation. So passive damping was employed which reduced deformation due to large stiffness, but too large damping forces enhance the response of upper structure therefore damping force must be controlled.

There are three broader types of damper named active, passive and semi- active damping devices. Active damping device was well facilitated by sensors and complete loop feedback control mechanism which was used to modify the damper according to need but they were exposed to damage and less reliable. Passive dampers cannot modify themselves according to need but were reliable and cost-effective with a little exposure to seismic fragility and can be easily replaced.

Liquid tuned damping LTD and magneto-rheological MRD damping have key issues of fluid leakage. They have high cost and low reliability as well, so the researchers moved towards metallic damper having large restoring force and deformation capacity and good low cycle fatigue. Number of loading cycle has a strong relation with maximum strain. A 3D CAD model is shown with meshed elements in fig 7
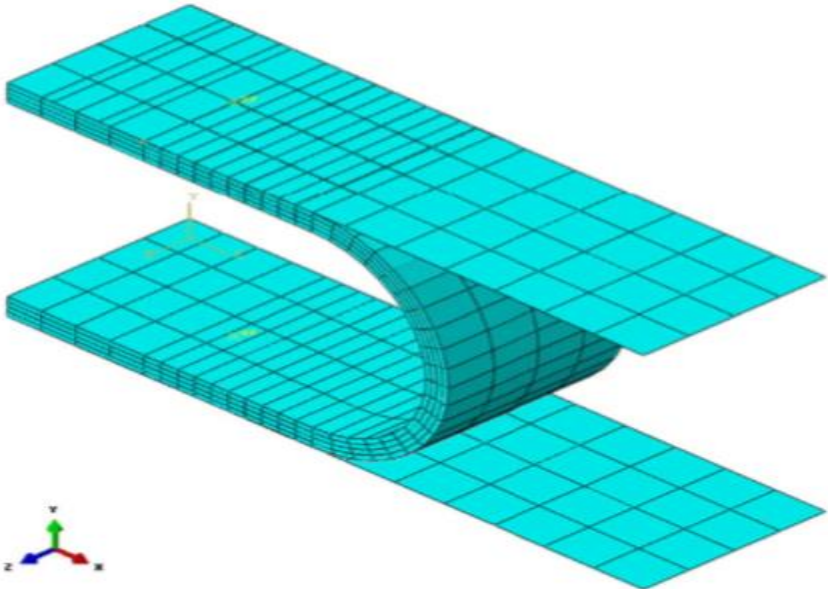
Figure 7: Dissipation Plate with connection plates assembly

While the dimensions of the damper in order to develop the mathematical model are shown in fig 8
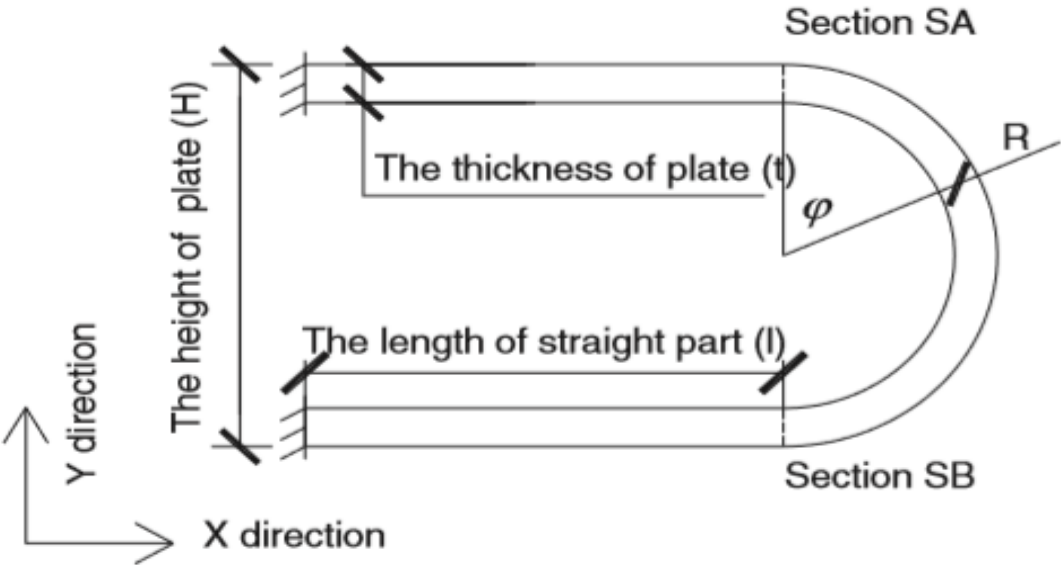
Figure 8: Dimensions of Dissipation plate

Basic equations for rotation angles are given below as

$$\theta_1 = \frac{1}{EI} \int_0^l (M + Qx)\,dx \tag{10}$$

$$\theta_2 = \frac{1}{EI} \int_0^\pi Q(l + R\sin\varphi)R\,d\varphi + \frac{1}{EI} \int_0^\pi [M - NR(1 - \cos\varphi)]\,d\varphi \tag{11}$$

$$\theta_3 = \frac{1}{EI} \int_0^l [M - 2NR + Q(l - x)]\,dx \tag{12}$$

$$\theta = \theta_1 + \theta_2 + \theta_3 = 0 \tag{13}$$

Where M, N, Q are the section moment, axial force and shear force of section SA, $H = 2R + t$. Now the basic equation for vertical and horizontal displacement by v and u respectively as

$$v_1 = \frac{1}{EI} \int_0^1 (m + Qx)x\,dx \tag{14}$$

$$v_2 = \frac{1}{EI} \int_0^\pi \{M(l + R\sin\varphi) + [Q(l + R\sin\varphi) + NR(\cos\varphi - 1)](l + R\sin\varphi)\}R\,d\varphi \tag{15}$$

$$v_3 = \frac{1}{EI} \int_0^l [M - 2NR + Q(l - x)](l - x)\,dx \tag{16}$$

$$v_4 = \frac{1}{EA} \int_0^\pi (Q\sin\varphi + N\cos\varphi)\sin\varphi R\,d\varphi \tag{17}$$

$$v_5 = \frac{1}{GA} \left[2\int_0^l Q\,dx + \int_0^\pi (Q\cos\varphi - N\sin\varphi)\cos\varphi R\,d\varphi \right] \tag{18}$$

$$v = v_1 + v_2 + v_3 + v_4 + v_5 = 0 \tag{19}$$

$$u_1 = \frac{2}{EI} \int_0^l [2NR - M - Q(l - x)]R\,dx \tag{20}$$

$$u_2 = \frac{1}{EI} \int_0^\pi [Q(l + R\sin\varphi) + M - NR(1 - \cos\varphi)](\cos\varphi - 1)R^2 d\varphi \tag{21}$$

$$u_3 = \frac{2}{EI} \int_0^l [2NR - M - Q(l - x)]R dx \tag{22}$$

$$u_4 = \frac{1}{GA} \int_0^\pi (-Q\cos\varphi + N\sin\varphi)\sin\varphi R d\varphi \tag{23}$$

$$u = u_1 + u_2 + u_3 + u_4 = \Delta \tag{24}$$

Now solutions for bending, shear force and axial force by solving above equations are given as

$$N = \frac{2\Delta E b t^3}{48lR^2 + 12\pi R^3 + 4lt^2 + \pi R t^2 (3 + 2\mu)} \tag{25}$$

$$Q = 0 \tag{26}$$

$$M = \frac{2\Delta E b t^3 R}{48lR^2 + 12\pi R^3 + 4lt^2 + \pi R t^2 (3 + 2\mu)} \tag{27}$$

The equations for maximum stress, yield stress, strength and ultimate strength is calculated as

$$\sigma_{max} = \frac{M}{I} \times \frac{t}{2} + \frac{N}{A} = \frac{N(6R + t)}{bt^2} \tag{28}$$

$$F_y = f_y \frac{bt^2}{6R + t} \tag{29}$$

$$F_u = 2F_{u1} = f_y \frac{t^2 b}{2R} = f_y \frac{t^2 b}{H - t} \tag{30}$$

There are four different types of damper created

Major parameters of specimens.

	H(mm)	t(mm)	Width(mm)	Remark
S1	300	16	200	Standard specimen
S2	300	16	200	Effect of connection plates
S3	300	25	200	Thickness of energy dissipation plate
S4	400	16	200	Height of energy dissipation plate

They are experimentally tested for which the coupon test gave the yield stress for structural steel is 280MPa while yield strain $1200u$. The simulation performed in ABAQUS and applied cyclic loading given by the fig 9
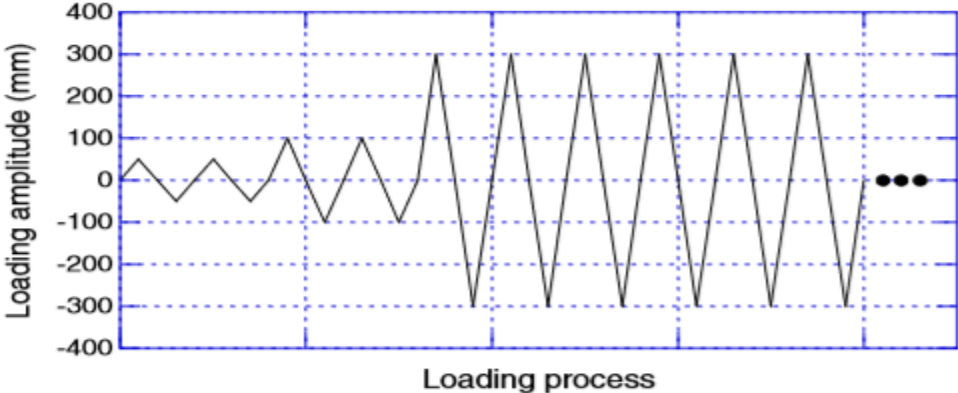

Figure 9: Cyclic Loading process

Hysteresis loops for four different kind of damper in fig 10 Mesh for whole model contained 980 elements with C3D8R for dissipation plate and R3D4 for connection plate assembly.
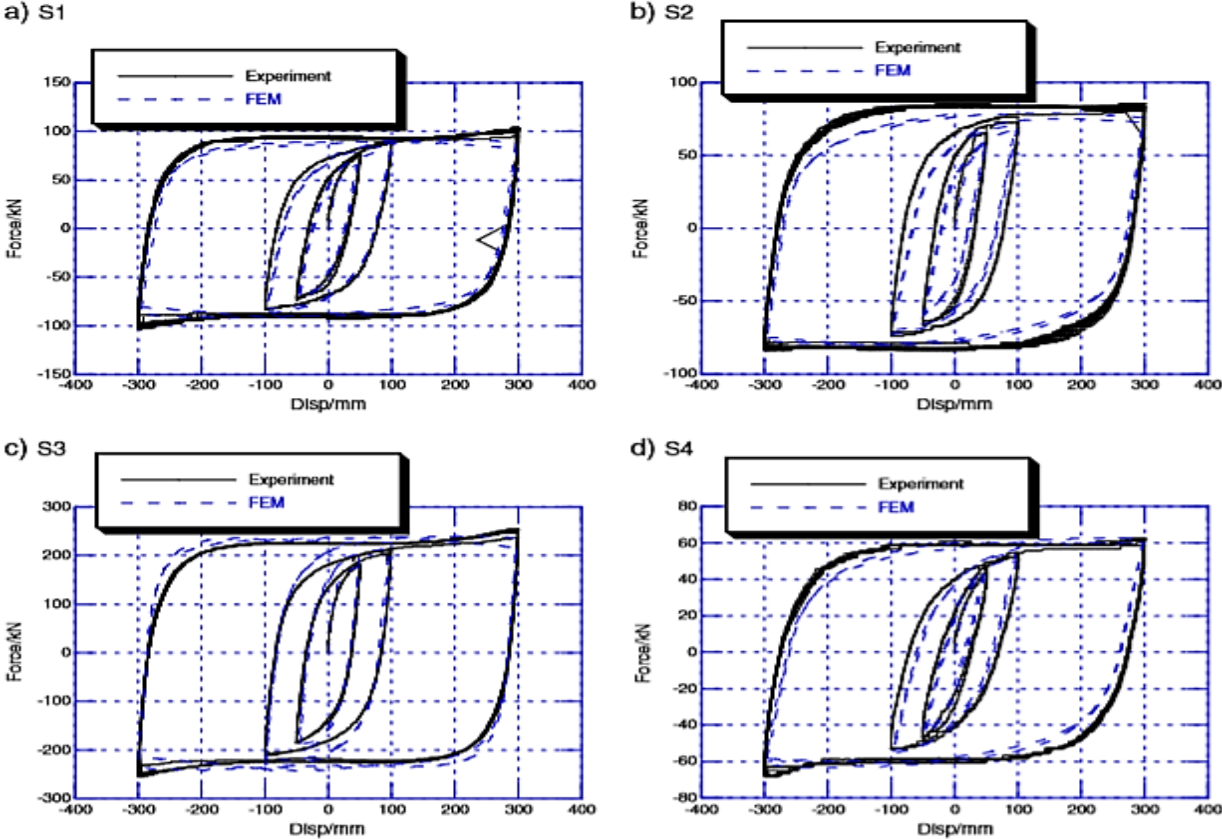
Figure 10: Stabilized cyclic responses for different parameters of dissipation plate

The effect of 3 back stresses are considered using CABOCHE hardening. The results revealed that by increasing the thickness of dissipation plate the ultimate strength is increased while it decreases by increasing the height of damper, but the effects are inverted for low cycle fatigue. The ultimate strength of damper was calculated with accuracy due to isotropic and kinematic hardening effects. Low cycle fatigue showed average life for all the types is 13 cycles.

2.3 Effect of viscous bridge damper on wind-seismic vibrations

This paper discussed that for long span cable stayed bridges omni-directional wind-tunnel aeroelastic tests revealed that the viscous damper had slightly damped the wind vibration and hence a very little effect on vertical buffeting of girder. The bridge must be designed separately for seismic and wind vibrations without considering effects of viscous damping. The damping of the bridge was improved by bride correctional aerodynamics, increasing the overall stiffness of damper and addition of material or structural damping. TMD were chosen as effective remedy for wind vibrations.

Hangzhou bridge used 8 nonlinear viscous dampers while 4 viscous dampers in order to check influence of viscous damping on wind-resistance phenomena. According to the mathematical relation

$$F = cv^\alpha$$

Where c is damping coefficient, α is damping index and v is relative velocity between damper ends. When $\alpha = 0$ the damper is friction, $\alpha = 1$ the damper is linear viscous, $0 < \alpha < 1$ the damper is nonlinear viscous. 18 different test cases were studied according to wind yaw angle, longitudinal, transverse and position of viscous dampers in table 2

Return period	ID	Earthquake	M	r	SF	Record	Soil
100 years	1	Izmit	7.8	77	1	1251	soft soil
	2	Montenegro (aftershock)	6.3	9	1	230	stiff soil
	3	Vrancea	5.8	77	1	6773	–
	4	Umbria Marche	5.5	3	1	591	stiff soil
	5	Alkion	6.7	10	1	333	soft soil
	6	Umbria Marche	5.9	4	1	594	rock
	7	Friuli (aftershock)	6	9	1	147	stiff soil
	8	Alkion	6,7	8	1	334	soft soil
	9	Umbria Marche	5.9	3	1	592	stiff soil
	10	Friuli (aftershock)	6	9	1	146	stiff soil
500 years	1	Duzce 1	7.3	0	1	1703	soft soil
	2	Montenegro	7	9	1	197	stiff soil
	3	Duzce 1	7.3	18	1	1560	soft soil
	4	Gazli	7	4	1	74	very soft soil
	5	Montenegro	7	12	1	199	stiff soil
	6	Izmit	7.8	5	1	1257	soft soil
	7	Izmit	7.8	12	1	1226	soft soil
	8	Izmit (aftershock)	5.8	5	1	6386	–
	9	Tabas	7.4	3	1	187	stiff soil
	10	Izmit (aftershock)	5.8	16	1	6383	–
1000 years	1	Izmit (aftershock)	5.8	5	1.85	6386	–
	2	Manjil	7.5	92	3.76	480	soft soil
	3	Montenegro	7	9	2.83	198	rock
	4	Izmit	7.8	97	2.35	1249	soft soil
	5	Dinar	6	0	1.67	879	soft soil
	6	Campano Lucano	6.9	13	2.57	291	stiff soil
	7	Kalamata	5.8	0	3,31	414	stiff soil
	8	Erzincan	6.9	1	1.1	535	stiff soil
	9	Kalamata	5.8	0	2.29	413	stiff soil
	10	Vrancea	6.9	51	2.94	6757	–

Table 2: Test case developed with varying yaw angle, number of dampers and their position

Wind velocities form 0m/s to 12m/s were applied with increment of 1m/s with cyclic application. Before excitation of the bridge in wind tunnel deformations and strains were measured to check plastic deformations to the model. The plastic deformation occurred at different frequencies caused a displacement of 10mm at different frequencies shown in fig 11
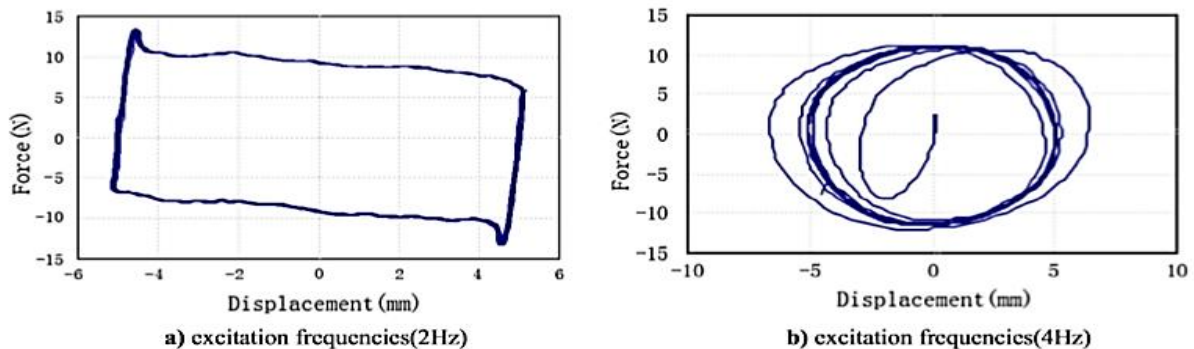

Figure 11: Hysteresis loop for flexural and torsional modes

This analysis revealed that torsional stiffness of bridge is large and vertical and lateral buffeting dominates and bridge performance depended upon lateral and vertical vibrational modes. Full aeroelastic model of the bridge is shown below in table 2.3

Dynamic characteristics of the full aero-elastic bridge model.

Vibration modes of girder	Theoretical bridge Freq. (Hz)	Theoretical model Freq. (Hz)	Measured model Freq. (Hz)	Error (%)	Damping ratio (‰)
Longitudinal floating	0.120	1.20	1.400	16.67	8.16
1st symmetric vertical	0.372	3.72	3.516	-5.48	7.13
1st anti-symmetric vertical	0.511	5.11	4.703	-7.96	7.30
1st symmetric lateral	0.483	4.83	4.224	-12.55	5.25
2nd symmetric vertical	0.742	7.42	6.729	-9.31	6.60
1st torsional	0.959	9.59	11.201	16.80	7.47

Table 3: Damping ratio with theoretical and simulation results of frequency

2.3.a   Analysis of buffeting response

Vertical mid-span bridge displacement with and without dampers are considered and compared. Longitudinal viscous damper responded positively but slightly as low as 3%. If the damping coefficient was increased damping increases but a limit came when damping coefficient did not influence damping and when it increased further after stable limit damping was reduced and when the damping coefficient was infinite damping was completely lost. A very small damping coefficient was almost had no damping effect. The value of reduced damping amplitude achieved was as high as 6% and occurred when the yaw angle was 60^0. By increasing the value of damping index α vertical mid span displacement and damper output was large and the reaction force on the structure would increase and structure response was enhanced. Longitudinal vibrational displacement of girder was due to vertical bending mode of girder. At last researchers concluded that wind-resistant and seismic resistant design was necessary rather to include viscous damping.

2.4   Kinematic hardening model for directional response

This paper postulated that Asymmetric plasticity, anisotropic yielding, early-reyielding, Bauschinger effect occurred simultaneously. Kinematic hardening model described before explained asymmetric plasticity of ductile metallic sheets behavior during cyclic loading at fixed single angle from rolling direction but unable to describe anisotropic hardening because parameters for kinematic hardening was for a reference direction. A condition function was generated and combined with kinematic hardening to incorporate the effect of different directions $0^0, 45^0, 90^0$.

Translation of yield surface captured effect of asymmetric plastic behavior which was further incorporated by back stress

2.5   Shear bending combined metallic damper

Normally these dampers were made *I* section where web plate was used to dissipate energy under shear loading while flanges provides end restraints. Optimal and economical usage of metallic material by flexural yielding which increases with the height of the plate. These kind of bending metallic dampers include set of parallel plates XADAS, TADAS, RADAS and HADAS. Shear metallic damper is less stable than bending metallic damper. But the strength and stiffness of SMD are greater than bending type. When X shaped plates were placed outside web plates so that shear and bending worked independently but out of plane buckling, pinching occurred.
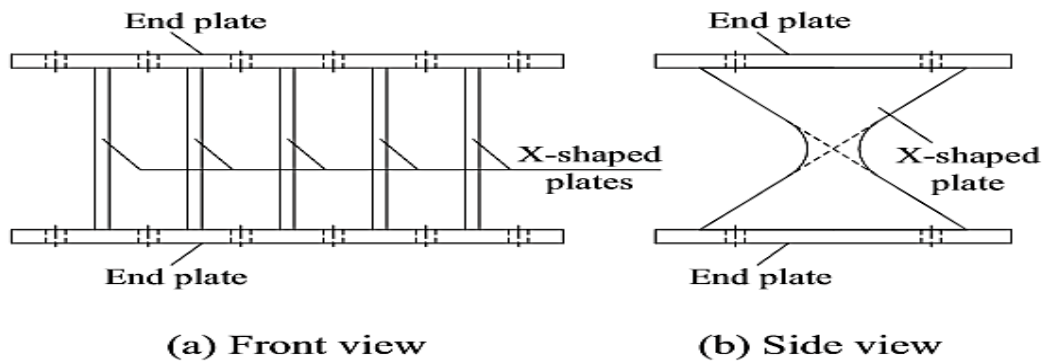

Figure 12: Front and side view of Shear-Bending combined metallic damper

But when the X plates were placed by partition by web so that two K shapes were formed and out of plane buckling was restricted by was restricted by K plates and now in-plane shear plastic deformation occurred while K plates have out of plane bending plastic deformation. SBCD improved energy dissipation capacity, stiffness, strength with improved stability. Force displacement relation for these types are given below in fig 13
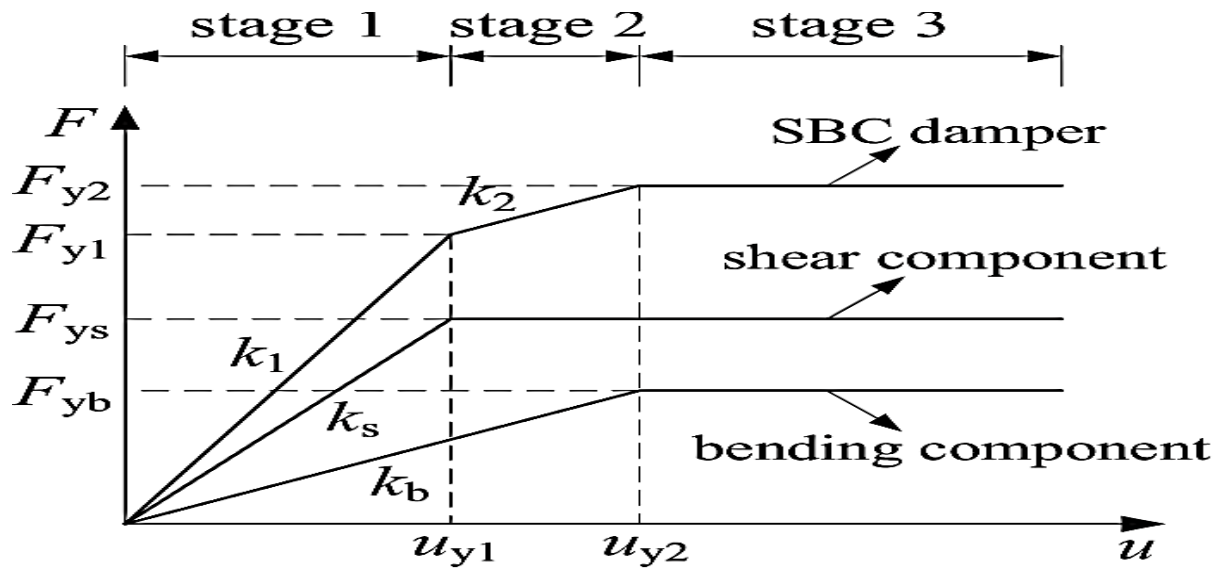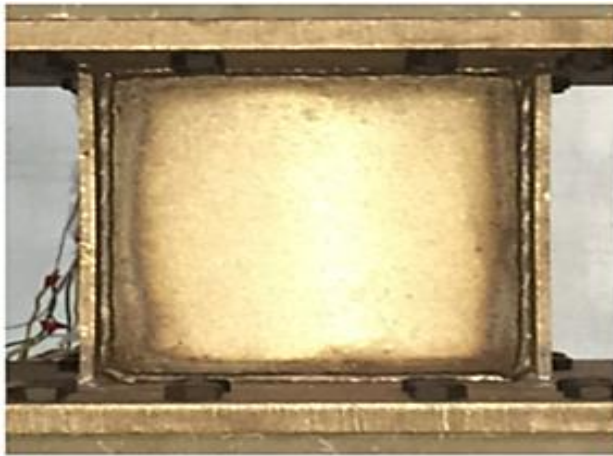
Figure 13: Force-Displacement graph of Shear-bending combined damper, flexural and shear damper

(a) Specimem-1
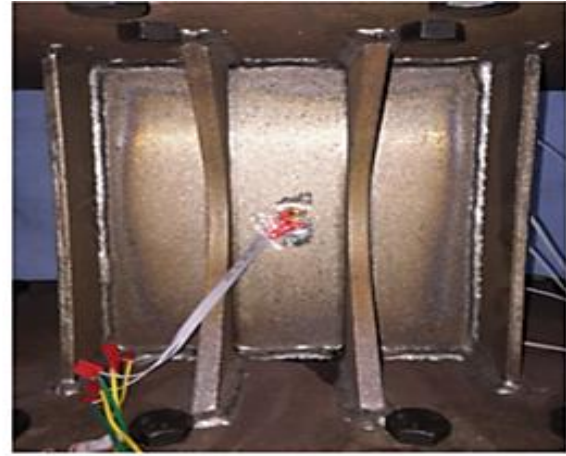
(d) Specimem-4

Figure 14: Shear bending combined metallic damper(d) and flexural damper(a)

Specimen 1 is with I section bending plate while specimen 4 is with XADAS with I bending plate. The hysteresis loop of specimen 1 and specimen 2 are shown as below with clearly shown larger hysteresis loop area for SBCD as compared to SP.
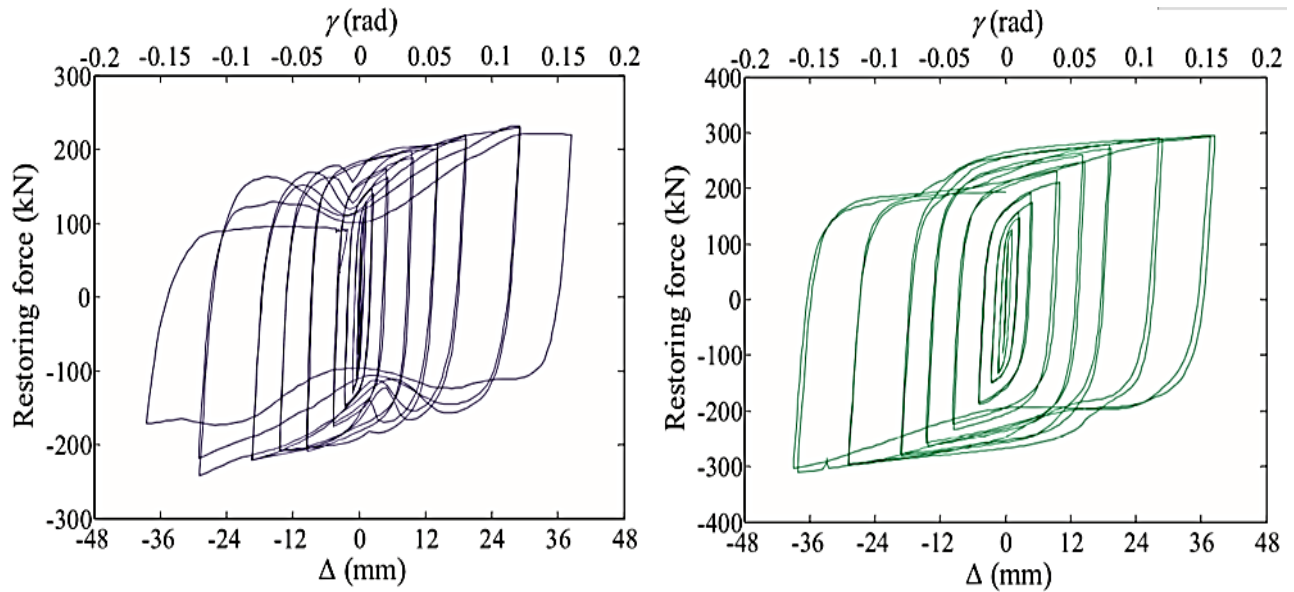
Figure 15: Hysteresis loop of Shear bending combined damper (d) with flexural plate (a)

A very slight pinching, buckling and crack growth failure was observed in SBCD as compared to SP. The summation of hysteresis energies of components of SBCD was less than SBCD. Smaller the gap between web plate and K plate improved hysteretic behavior but the friction between both the plates exposes the SBCD to damage which can be improved by applying protective coating. 3D view of SBCD in fig 16
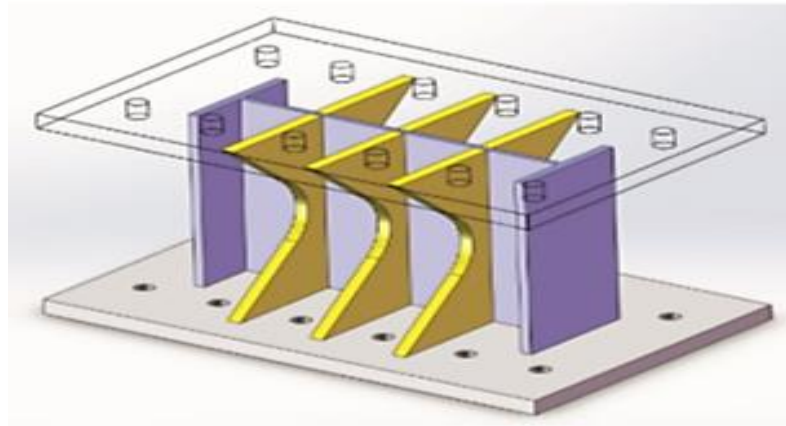
Figure 16: 3D view of Shear-bending damper

2.6   Piston Metallic Damping

The damper studied in this research dissipated energy by flexural and tensile yielding. At small displacements flexural yielding occurs while at large displacements tensile yielding occurs. The hysteresis loops obtained were stabilized with no stiffness and strength degradation. This damper had good ductility and stiffness. Its stiffness and strength increased at larger strains and it has high strength to weight ratio. Section view is shown

below in diagram with useful dimensions in fig 17

Figure 17: Sectional view of piston metallic dampers

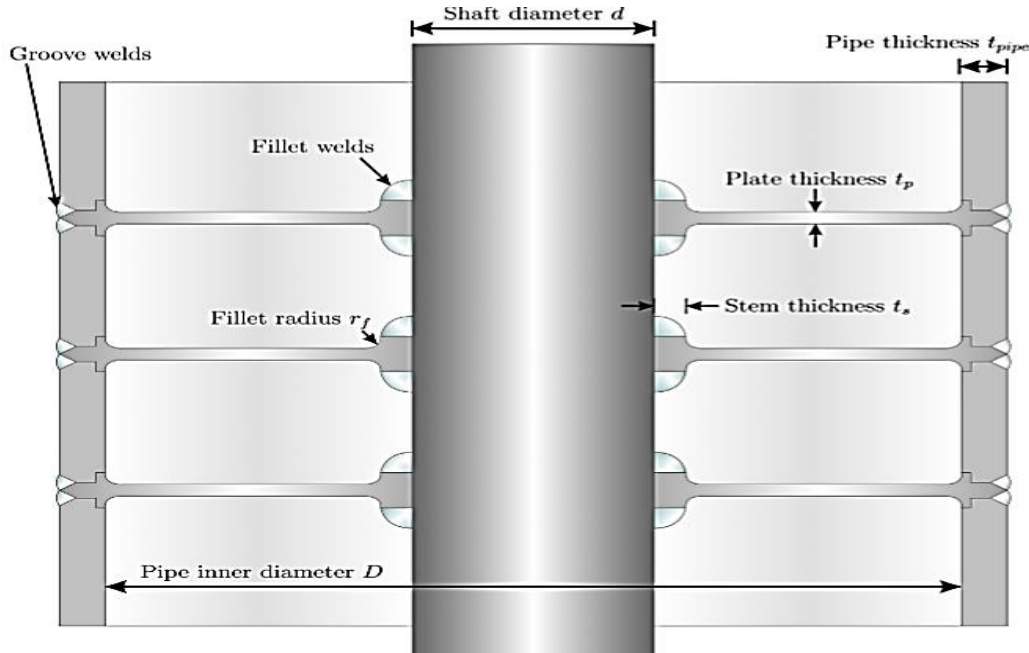The experiments were performed for monotonic and cyclic loading and the results are compared with the ABAQUS 6.14.1 simulation results. Researchers founded that cumulative dissipated energy is approximately equal to monotonic curve for total applied strain. The dissipation energy is not affected by strain rate as it only depends upon the applied strain. With low shaft to pipe diameter ratio butterfly shape loops are obtained which shows low dissipated energy while the loops with high shaft to pipe diameter ratio shows rectangular loops with high energy dissipation capacity. Yielding is not affected by number of numbers of annular plates.

Material properties of plates.

Steel types	Young's modulus E (GPa)	Yield stress σ_Y (MPa)	Ultimate stress σ_u (MPa)	Failure strain (%)
St-1	203	278	453	35
St-2	203	305	473	31

Table 4: Material properties of mild- steel
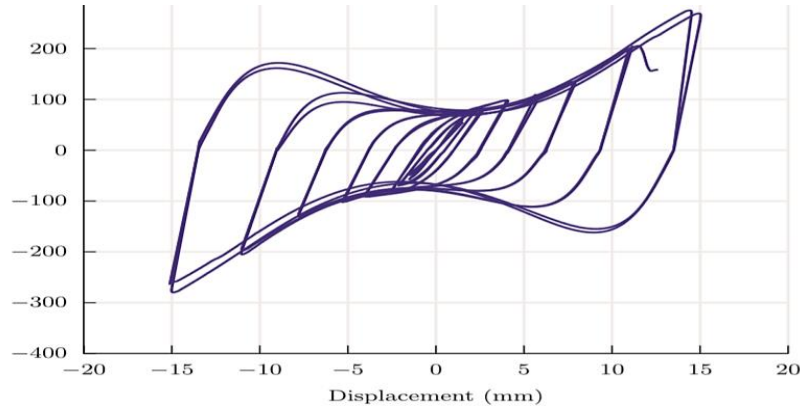
ABAQUS simulation results in figure 18

Figure 18: ABAQUS Simulation nodal responses of piston metallic damper

Damper endured 24.5 to 53 KJ of energy and endured cumulative displacement of 400mm During low cycle fatigue analysis, the stress concentration factor in the inner edge of the plate decreased the fatigue life. Load history is comprised of 0.5, 0.1, 0.3 and 5 amplitude set with repetition for 5 cycles at 10mm and 15mm. No damage occurred for first 5 cycles for 10mm while plate got fractured at the end of second cycle and crack slowly starts initiated for the start of second cycle. This was in accordance with ASCE7-10 standard for the displacement of 10mm in which plate survived 5 cycles. The damper is like ADAS and The mathematical model used to calculate the stiffness of damper for different shaft diameter to pipe ratio is as

$$K^i_{eff} = \frac{\mid P_{i,\,max} \mid + \mid P_{i,\,min} \mid}{\mid \delta_{i,\,max} \mid + \mid \delta_{i,\,min} \mid}$$

Elastic stiffness and first yield point have linear dependence.

2.7 Hysteretic damper for buildings

Efficiency of system including damper and building is affected by yield strength, yield displacement and brace-damper stiffness. Hysteretic steel damper was cost effective and capable to dissipate energy by its low yield strength and large rupture strain, this all was associated with ADAS. As far as seismic uncertainties were studied, two buildings were designed according to European code and uncertainty was studied with optimized Latin Hypercube Sampling. Annual seismic damage frequency was quantized by seismic fragility and hazard curves. Yield displacement, yield force and stiffness ratio were affected 10 storey building structural response. Friction plate damper is shown in fig 19
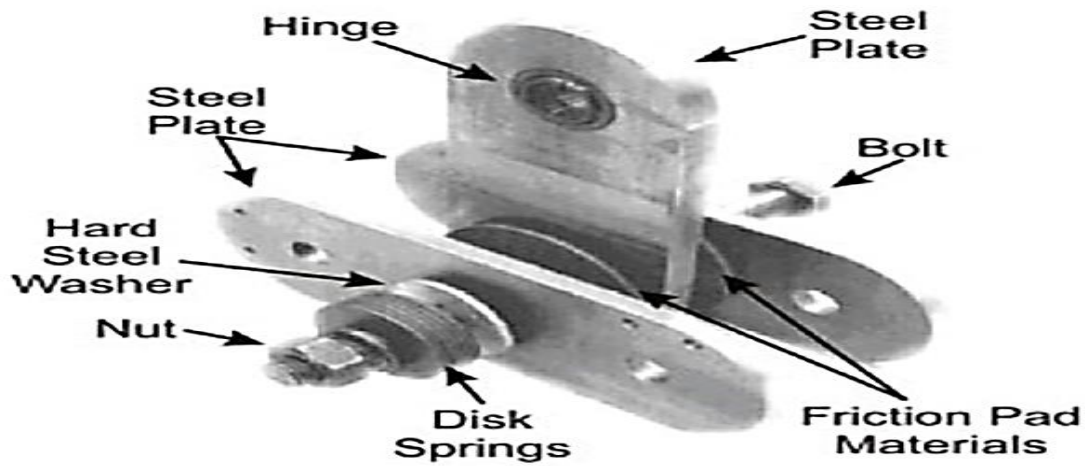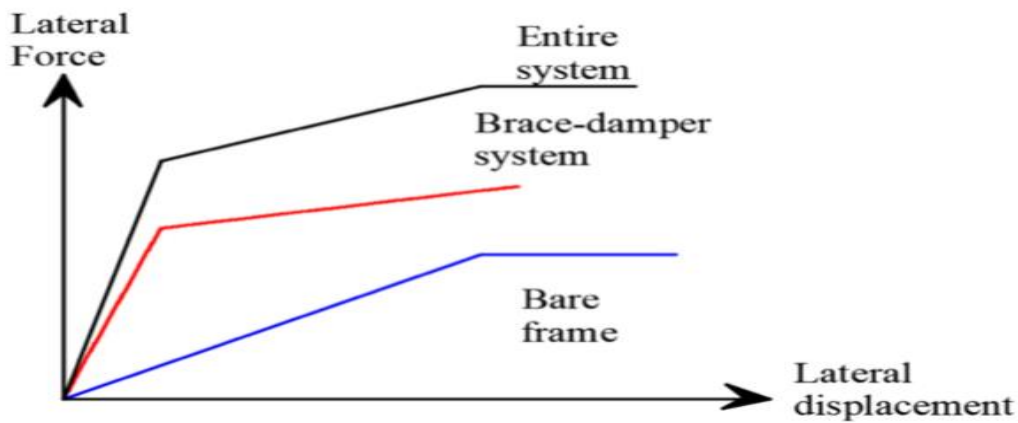
Figure 19: Frictional steel plate damper for buildings

The power law to predict the annual hazard using curve fitting technique was formulated as

$$\nu_{S_a(S_r)} = k_0 S_r^{-k_1}$$

Where $\nu_{sa(sr)}$ was considered as annual probability of first mode spectrum s_a. The model covered fragility for 100, 500, 1000-year return period.

ADAS damper was inefficient at low seismic intensities concluded from interstorey drift distribution while it was effective for moderate to high seismic levels. Large dispersion was observed using uncertainty parameter and conclusion made were not so applicable. The study was only valid for one dimensional 2D frame and not for 3D model.

2.8 Low cycle fatigue and plasticity

Low cycle fatigue was measured for mid steel experimentally and numerically. Mild steel was still used in market because of low yield, softness, malleability, ductility and work hardening but low ultimate strength with less corrosion resistance. Cyclic stress-strain relationship with NLCHM was performed in ABAQUS. A hysteresis loop given below in fig 20 with elasto-plasticity is shown with tensile test specimen
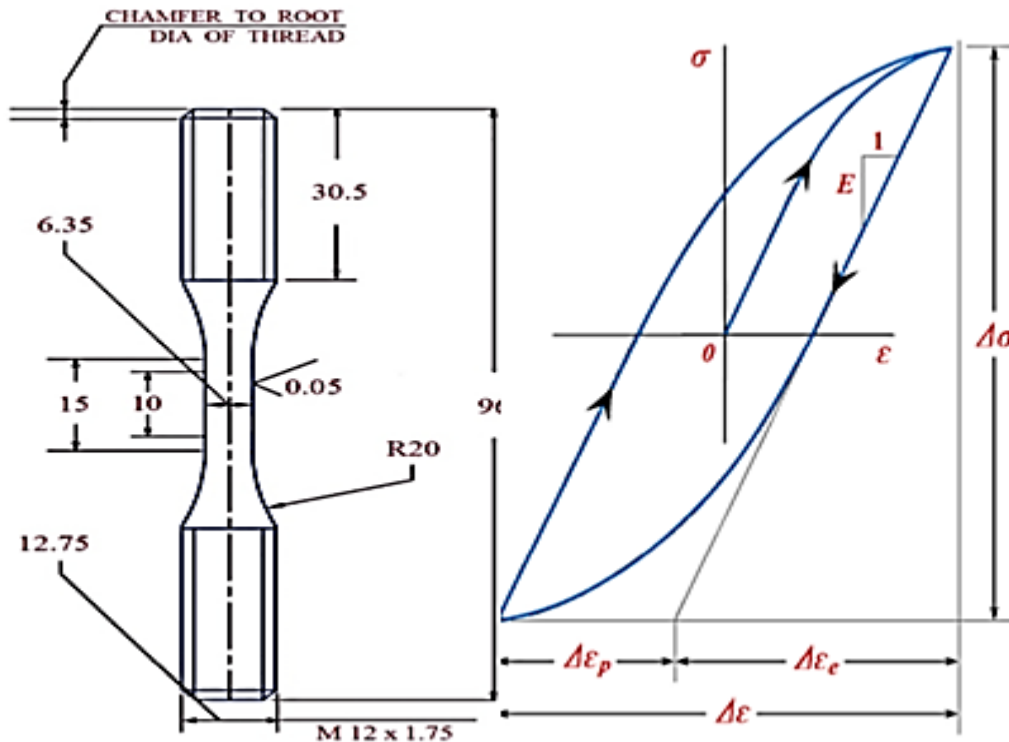

Figure 20: Total strain for first yield cycle for Bone-shape specimen

Above specimen was loaded cyclically using servo-hydraulic test system and constant strain amplitudes of $\pm6\%$, 8%, 1%, 1.2% were applied for four different specimens here Consider only 6% strain case in order to calibrate NLCHM. The specimen got failed by fatigue where the crack initiated at microscopic level with sudden loss of load resistance. When half number of total loading cycles to failure $\frac{N_f}{2}$ occurred, the loop became stabilized and invariant. The loop got stabilized at data point $\left(\frac{\Delta\varepsilon}{2}, \frac{\Delta\sigma}{2}\right)$ from CSS life. $2N_f$ cycles load reversals were necessary to get fatigue fracture. Strain life calculated by using Basquin-Manson-Coffin Relation

$$\frac{\Delta\varepsilon}{2} = \frac{\Delta\varepsilon_e}{2} + \frac{\Delta\varepsilon_p}{2} = \frac{\sigma_f'}{E}(2N_f)^b + \varepsilon_f'(2N_f)^c$$

Where

Fatigue ductility coefficient, ε_f'	0.0304
Fatigue ductility exponent, c	-0.2782
Fatigue strength coefficient, σ_f'	606.09 MPa
Fatigue strength exponent, b	-0.0352

And these parameters were calibrated using non-linear regression by least square fit technique.
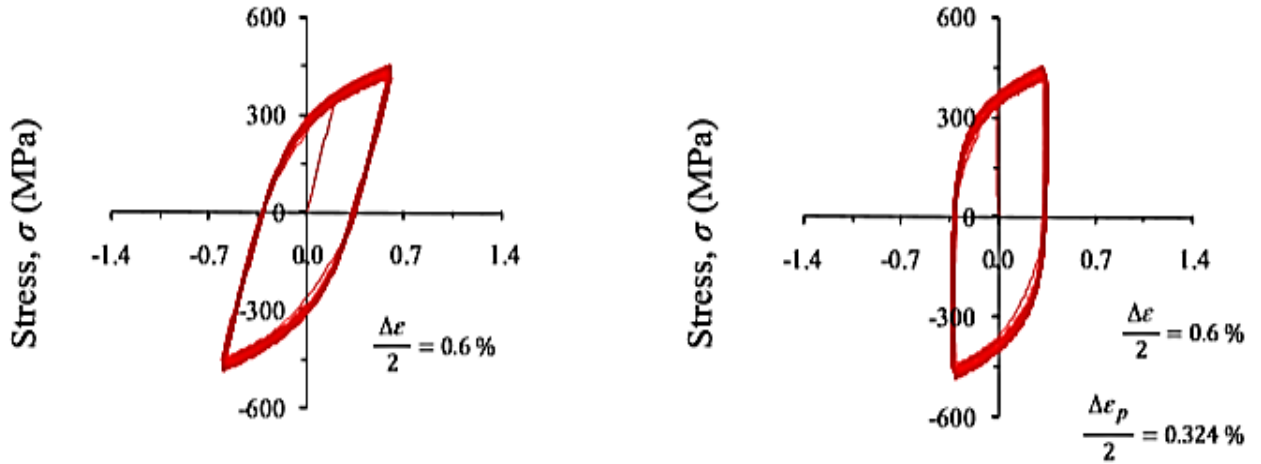

Figure 21: Stabilized Cyclic response for mild steel as Low cycle fatigue analysis

The above parameters were only for stabilized response. But before reaching such stability the loop was variant, refers to work hardening and softening by increase or decrease in load resistance due to imperfections in geometry. Leimatre and Chaboche developed combined hardening model for NLCH. So, for the ith cycle accumulated strain was linked with the total strain as

$$\varepsilon_i^{p,acc} = (4i - 3)\frac{\Delta\varepsilon_p}{2}$$

This plasticity model was quite handy and gave expansion and translation of yield surface which incorporated Bauschinger effect as well. Kinematic hardening increased at low strain amplitude and rate of hardening decreased with increased in strain amplitude.

CHAPTER 3

Creating 3D CAD model assigning properties and other modules for simulation

There are many SOFTWARES developed for creating CAD models and simulating by using FEA methods. The results are extracted from the nodal responses and the integration points available in ABAQUS SIMULIA 6.13.1. The software is used regarding steady state analysis as well as hysteretic analysis during cyclic loading of damper. The results are further analyzed by using MATLAB code for FRF in order to calculate damping ratio for the modal frequencies.

3.1   Creating 3D U-shape geometry of Steel and composite

U-shaped 3D steel model is created and properties of steel like density, elasticity and combined hardening parameters are applied while a separate polyurethane U-shaped laminate is made with properties of elasticity, density and loss factor in terms of real and imaginary is applied to specify both materials. Steel and polyurethane geometries with different types are shown in fig 22 the U-shape space is for placed laminate with different thickness
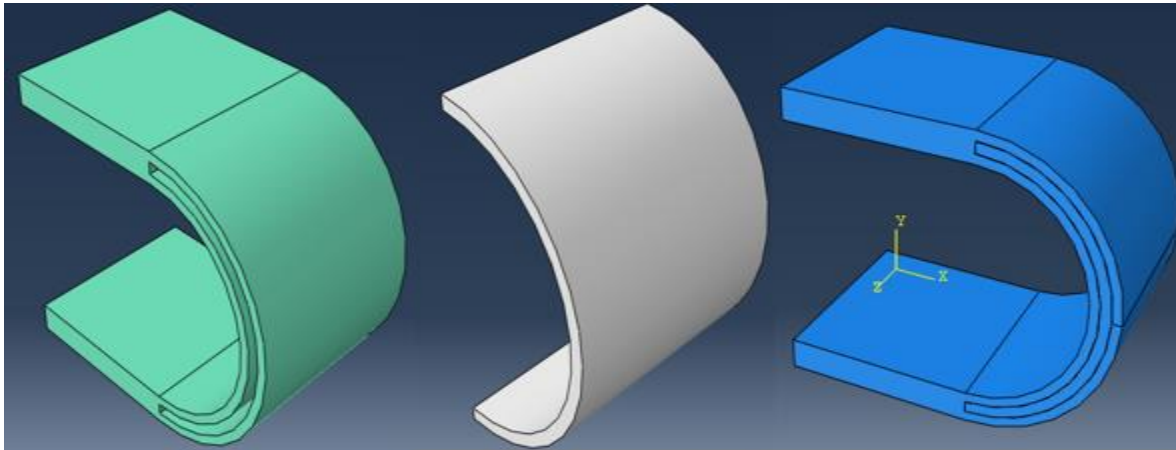

Figure 22: Dissipation plate with polyurethane laminate of white colour

Fig. 22 white with viscoelastic polyurethane, green with steel and blue with both assembled

Table 5 shown below has applied for isotropic hardening properties of structural steel with different geometries and boundary conditions

Yield stress(MPa)	Plastic strain
270	0
300	0.0025
330	0.0075
350	0.0125
370	0.0175
400	0.04

Table 5: Isotropic hardening properties of structural steel

$$\varepsilon_T = \sigma/E + \left(\frac{\sigma}{Ep}\right)^{1/n}$$

Where ε_T is the total strain with E as elastic modulus and Ep as plastic modulus and n is known as strain hardening exponent

Combined hardening parameters with 3backstresses for cyclic Reponses of structure are shown in table 6

C_1	γ_1	C_2	γ_2	C_3	γ_3	Q_∞	v
7×10^9	250	1.5×10^{10}	400	4×10^9	200	1.7×10^8	8

Table 6: Combined hardening parameters of structural steel

A mathematical model developed for the above parameters regarding cyclic plasticity

$$\alpha = \sum_{k=1}^{n} \frac{C_k}{\gamma_k}\left(1-e^{-\gamma_k \bar{\varepsilon}^{pl}}\right)$$

$$\sigma^0 = \sigma\big|_0 + Q_\infty\left(1-e^{-v\bar{\varepsilon}^{pl}}\right)$$

σ_0 has been considered as the initial yield of the material i.e. structural steel for very first cycle. ε^{pl} is the equivalent plastic strain. Q_∞ represented limit of isotropic hardening and may be positive or negative indicating cyclic hardening or softening. γ represented rate of kinematic hardening while α is the back stress. c_k and γ_k were obtained from stress-strain curve based on coupon test. The above model in cooperates effect of Bauschinger effect

The model applied for damping ratio has been represented by relation

$$\eta = 2\zeta$$

Where twice of damping ratio ζ equals loss factor η

$$m\ddot{x} + K \times (1 + i\eta) = Re\left(\dot{F}e^{i\omega t}\right)$$

$$\eta = {k''}/{k'} = \frac{E''}{E'}$$

$$E^* = E' + jE''$$

Where E' and E'' are storage and loss modulus while k' and k'' are real and complex part of stiffness. The loss factor for steel is 0.0001 while for polyurethane it is 1.

$\omega_R(g^*) = {E''}/{E_0}$ and $\omega_I(g^*) = 1 - {E'}/{E_0}$ are the loss parameters for ABAQUS as in fig 23 below

Figure 23: Viscoelastic properties for material damping

Interaction between the surface of polyurethane and structural steel is developed by using tie. Tie generates master surface for steel and slave for polyurethane. In order to transmit a vibration in the form of strain control model slender steel rods were made and two different boundary condition were tried for pure steel and its composite for Structural hysteresis and material damping

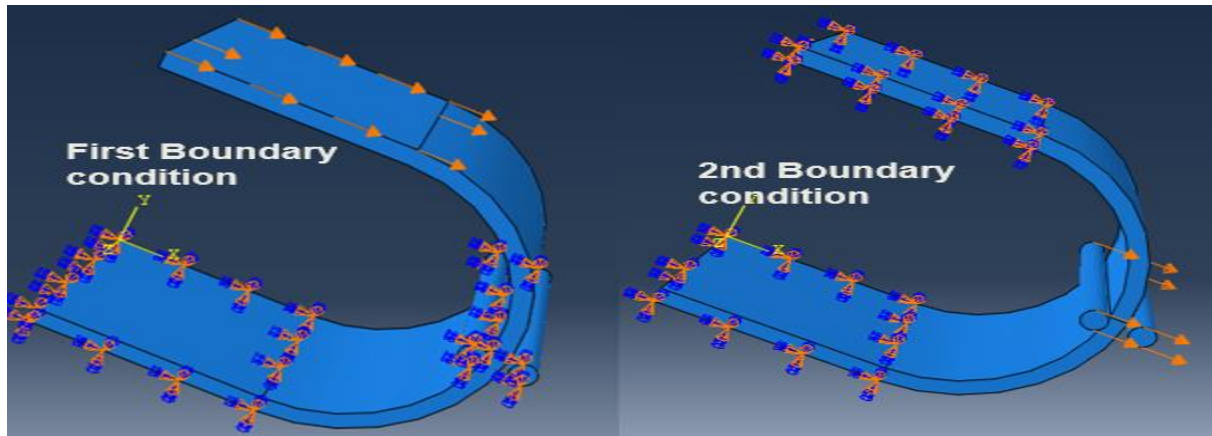Boundary condition 1 and boundary condition 2 are shown in figure 3.2 below

Figure 24: Dissipation plate with different boundary condition and assembly

Different types were generated with different laminate thickness, different material ratio and different thickness, boundary condition and parameters of steel shown in table 7

Types	Configurations	Boundary conditions
TYPE 1	r=7mm, total length=86.29mm, gauge length=40,effective gauge length=21mm, bell shap	B.C 0
TYPE 2	t=16mm, r=150mm, r=165.5mm, r=185.5mm No Polyurethane, steel rods, U-shape	B.C 1
TYPE 3	t=16mm, r=150mm, r=165.5mm, r=185.5mm No Polyurethane, steel rods, U-shape	B.C 2
TYPE 4	t=20mm, t=25, r =150mm, No Polyurethane, steel rods, U-shape	B.C 1
TYPE 5	t=20mm, t=25, r =150mm, No Polyurethane, steel rods, U-shape	B.C 2
TYPE 6	Steel base=17mm, laminate=1mm, concentraining layer=3mm,U-shape	B.C 1
TYPE 7	Steel base=17mm, laminate=1mm, concentraining layer=3mm, U-shape	B.C 2
TYPE 8	Steel outer layer=10mm, steel inner layer=10mm ,Laminate thickness = 5mm/9mm, U-shape	B.C 2
TYPE 9	Steel outer layer=10mm, steel inner layer=10mm ,Laminate thickness = 11.5mm, U-shape	B.C 2

Table 7: Different types of damper w.r.t material, dimensions, geometry and boundary condition

MATLAB code using half power point method to get damping ratio has been generated
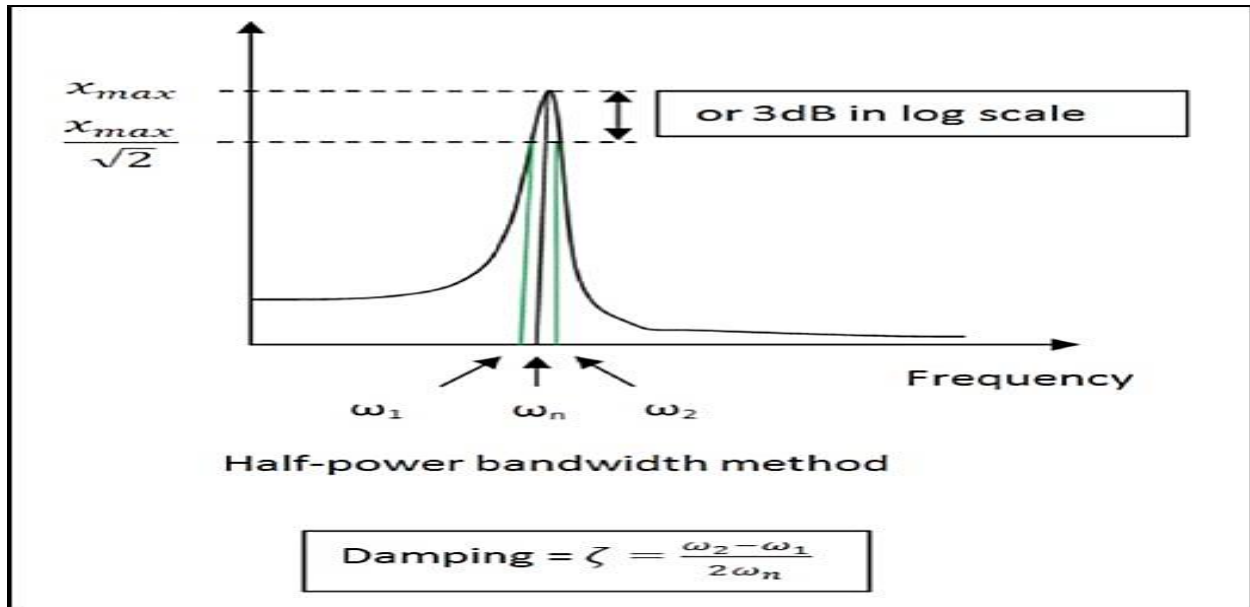

Figure 25: Half power point method

3.2 Generation of Step in ABAQUS

As far as steady state analysis is concerned linear perturbation is used with its subtype steady state dynamics direct if the modal frequency range is calculated from linear perturbation with its subtype frequency and first 5 modes are requested using eigen solver. These all are concerned with material damping.

While for structural hysteresis Static general step is created with time period of 16s which is the real time with specifying the increments of 10000000 and specifying increment size according to need of convergence by assigning values to initial, minimum, maximum. General solution manager is also modified according to need. Two steps are created with two different loops outer and inner loops.

3.3 Application of load

Load is applied according to the boundary conditions specified for both hysteretic as well as damping analysis but for all types of the U-shape dampers created. In first boundary condition lower end of steel, mid of the damper is fixed and upper end is applied displacement while in second boundary condition the upper and lower ends are fixed, and displacement control model is generated by applying displacement at the middle. Load of

100N is applied for steady state analysis. For hysteretic analysis displacement-controlled boundary conditions for the time of 16s are scaled by amplitude given as fig 26
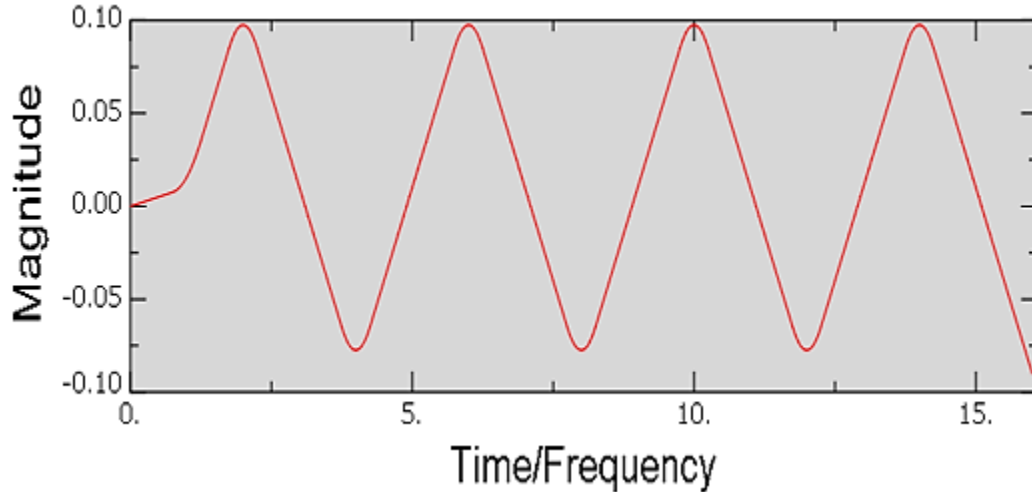

Figure 26: Scaling amplitude for cyclic displacement

3.4 Mesh Strategy in ABAQUS

After complicated assembly and developed interactions a mesh strategy of C3D8R, C3D8H and C3D20R are applied and mesh sensitivity is checked by achieving convergence. Fig 27 is showing mesh strategy regarding FEM
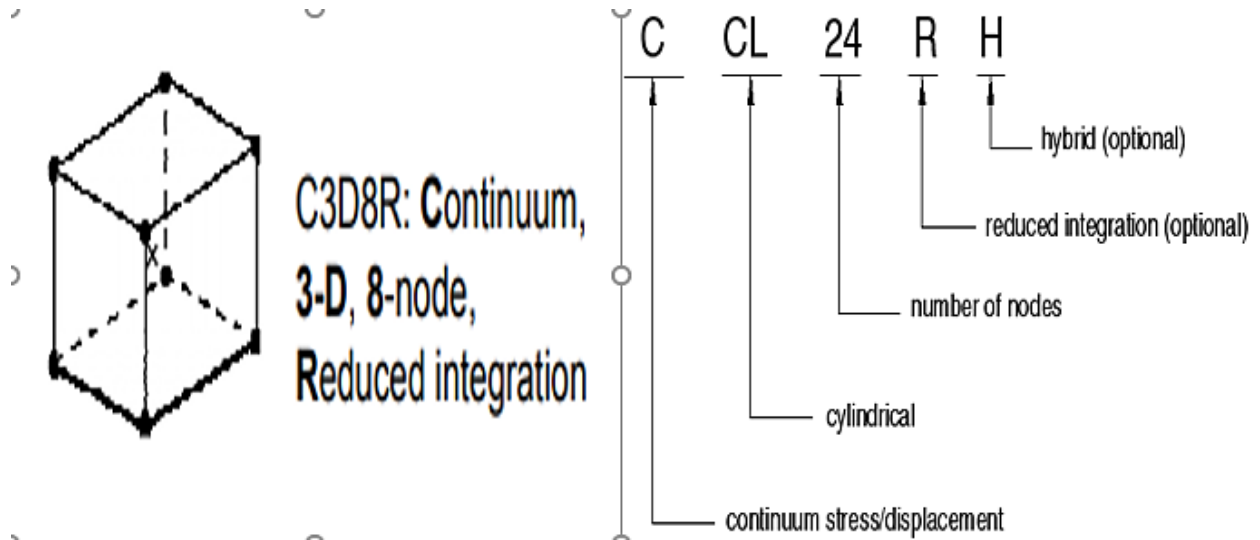

Figure 27: Mesh Strategy in ABAQUS

CHAPTER 4

CASE STUDY

This chapter deals with the case study of different parameters which includes different thickness, different radius, different length, different height, different volume, different mass of the damper. Study of different geometries includes bell shaped, U-shaped. Different boundary conditions of the previous research, different interaction with different assemblies are considered. First modal frequency

4.1   Previous Research Geometry

Previous researchers used simple bell-shaped geometry for analysis hysteresis energy by applying different boundary condition. The isotropic and kinematic hardening are analyzed separately as well as combined hardening is also applied then the numerical error is reduced by applying plasticity model. There are many drawbacks regarding this kind of geometry because of buckling and non-adoptability towards installation between pier and girder of the bridge. There is only uniaxial mode of yielding and plastic deformation beyond yield point, but no bending and torsion is incorporated. The cyclic responses yield lesser loop area, less stiffness, less resistance is offered against the applied load. Due to buckling it can only be applied for low seismic intensities only with less energy dissipation capacity and operable in very small applied displacement. Only be used for structural hysteresis while there is no material damping offered. Fig 28 with geometry 1 is below with previously used boundary condition
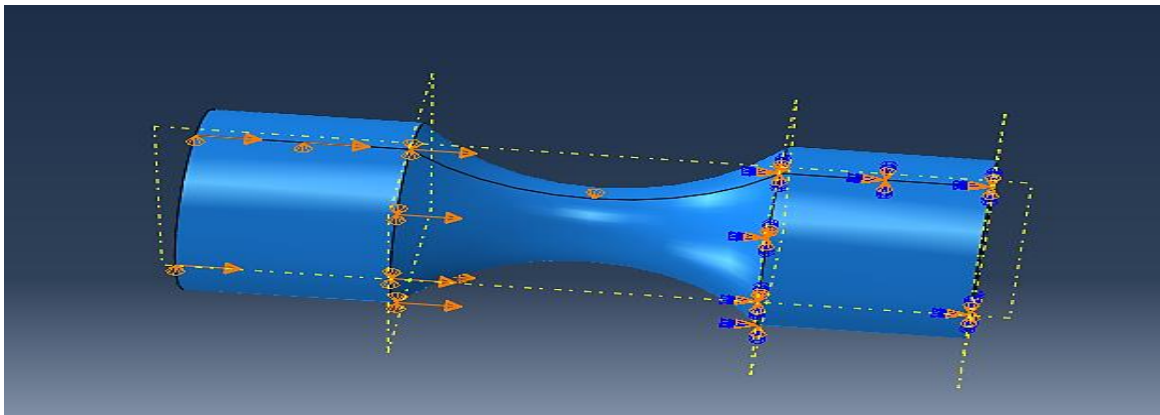

Figure 28: Simple tension test Specimen with applied boundary conditions

One end of this geometry is fixed and the other is moving. Orange colored arrow heads are showing axially applied displacements.

4.2 Current research geometries

New geometry is developed in order to eliminate the drawbacks of the previously developed geometry with different assembly, different boundary conditions, parameters and interactions. U-shape is developed in order to combine the effect of axial plasticity as well as bending induced yielding. The geometry is shown in fig 29
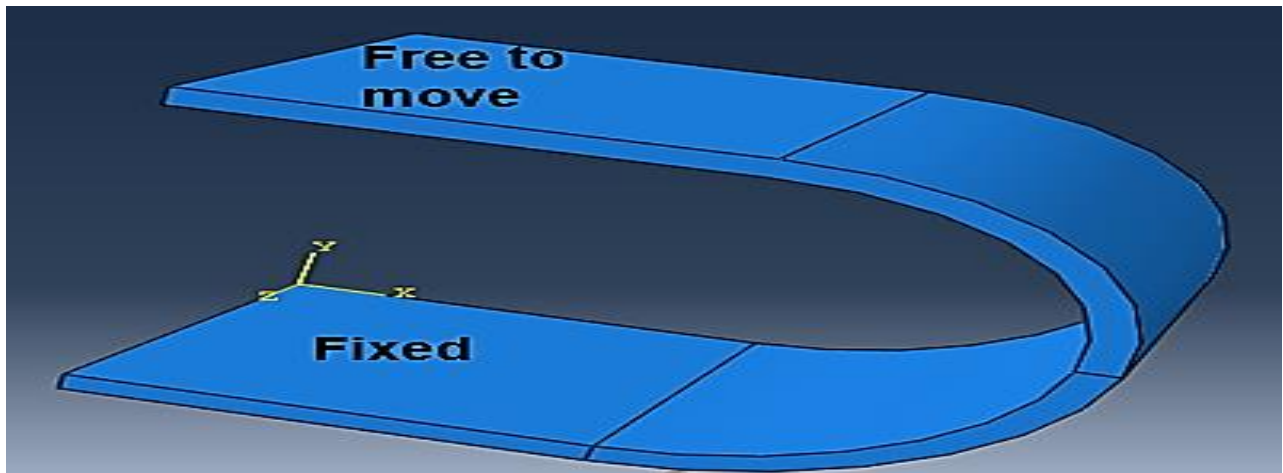

Figure 29: Previous boundary conditions for dissipation plates

This is also known as dissipation plates made of structural steel lower end of which is fixed while its upper end is moving. Combined effect enhances energy dissipation capacity at high seismic intensities but less sensitive towards moderate and high seismic intensities even at high seismic intensities a very a smaller number of active yield points are less and needed to be improved by assembled connection plates which are attached to the upper and lower end of the damper by using hard contact having coefficient of friction 0.3 in ABAQUS. Number of mesh elements are 980 and C3D8R is applied on dissipation plate while R3D4 for connection plates. A meshed connection plate assembly is shown in the figure 30 below
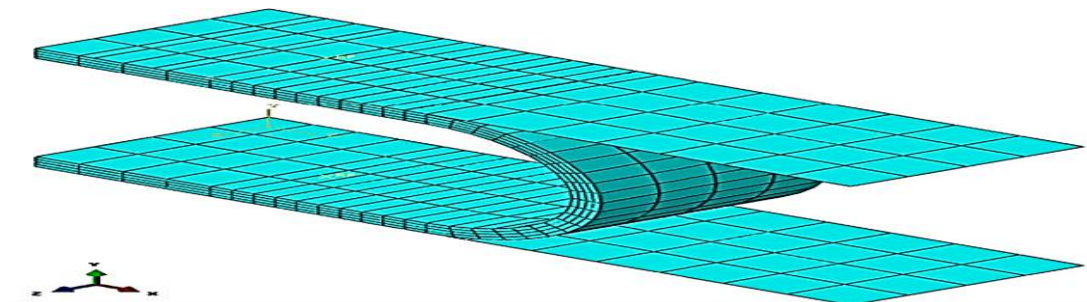

Figure 30: Case study of U-shape steel plate with connection plates

The damper responds at larger displacement of 50mm to 300mm for significant hysteresis shown

below therefore a modification is required such that sensitivity of damper is enhanced. Taken from paper as reference given below

Deng, K., Pan, P. and Wang, C. (2019). Development of crawler steel damper for bridges.

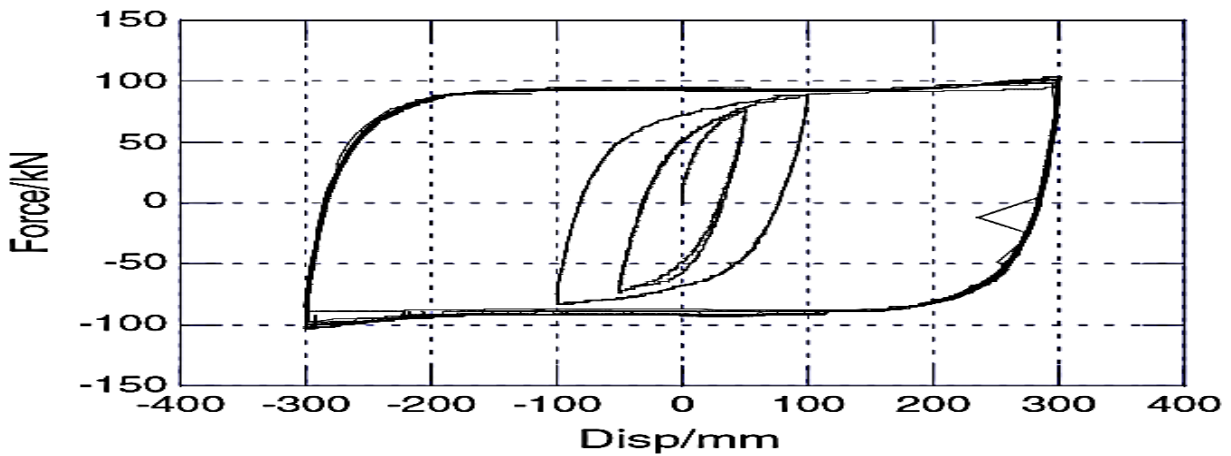## a) Hysteresis curve

Figure 31: Stabilized and saturated hysteresis loop for dissipation plate

4.3   Dynamic response of vehicle passing over the bridge

Passing vehicle on a bridge behaves as a vibration shaker and hence excites bridge. The bridge is considered as a simply supported beam and properties in table 8

L	25m
E	27.5GPa
M/L	4800 Kg/m
m	1200kg
k	296KN/m
I	$0.12m^4$
A	$2m^2$

Table 8: Material and structural properties of bridge and vehicle

For the above case when vehicle moves with velocity of 10m/s then no resonance occurs resonance occurs when it moves with velocity of 20m/s then shifted frequency of the bridge against the

dynamic response of vehicle is 2.48Hz while frequency of vehicle is 2.5Hz.Now a damper geometry, material and B. Cs are selected such that it is comparatively higher than the bridge and vehicle so as to avoid resonance. Increasing the stiffness will increase the first frequency of bridge hence increase the gap between bridge shifted frequency and vehicle frequency against resonance. Very high vehicle velocities are required i.e. above 20m/s response spectrum are plotted as the acceleration spectrum of vehicle bridge first modal frequencies which are higher when the vehicle is midway on the bridge. FRF for the vehicle bridge interaction are given in figure 32, 33 and the resonant case in figure 34 taken from research paper with reference as

Yang, Y., Lin, C. and Yau, J. (2004). Extracting bridge frequencies from the dynamic response of a passing vehicle. Journal of Sound and Vibration, 272(3-5), pp.471-493.
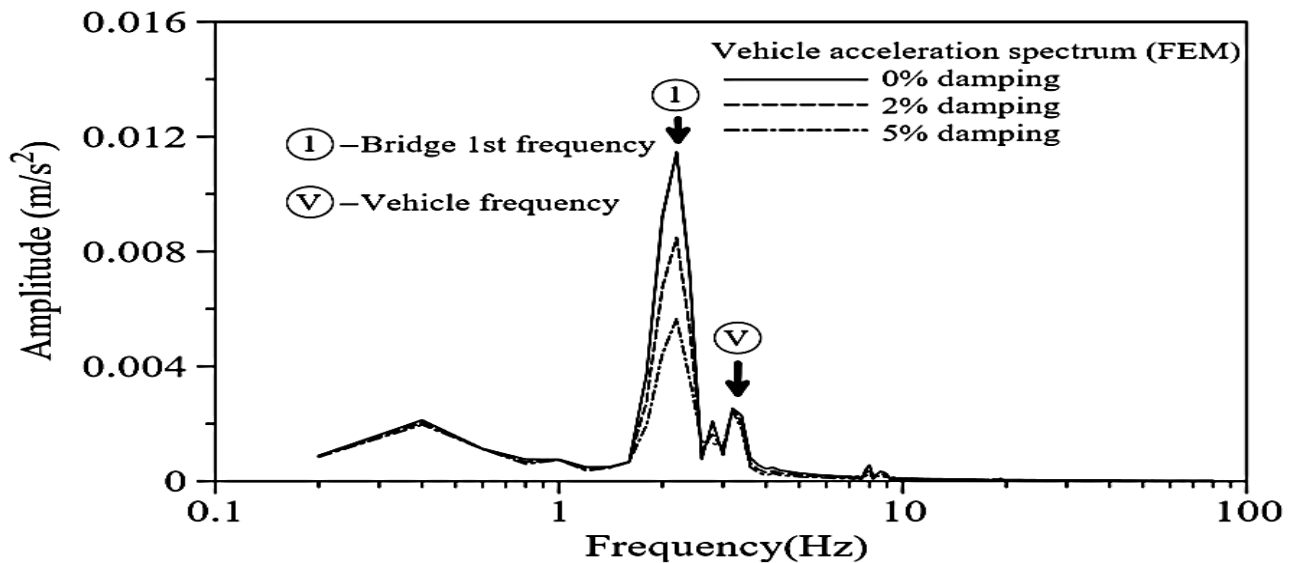

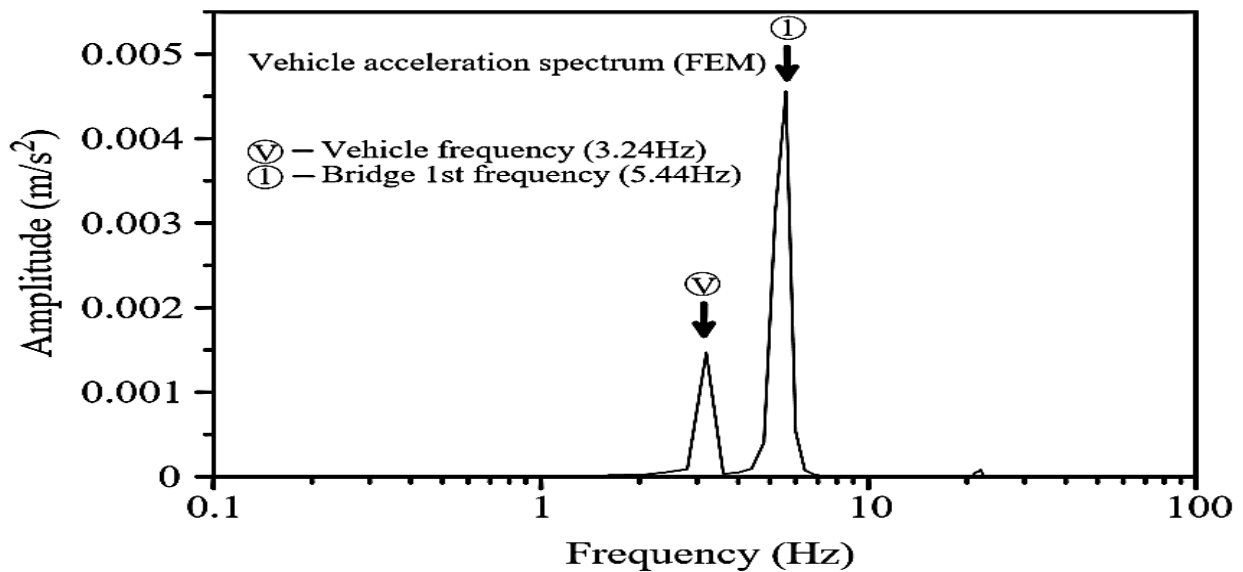*Figure 32: Effect of damping on vehicle bridge-frequency*
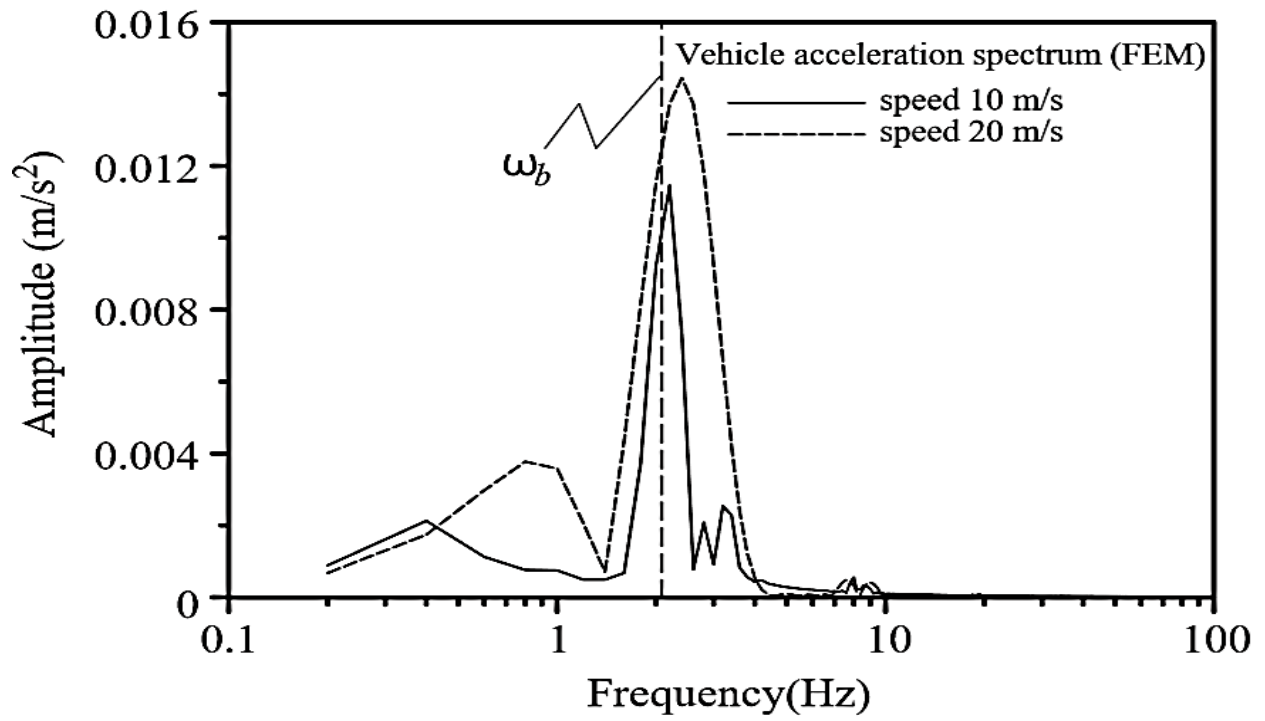

Figure 33: First modal frequency for stiffer bridge

Figure 34:Resonance due to Dynamic vehicle on bridge

CHAPTER 5

RESULTS and DISCUSSIONS

This section describes that there are 9 different types of damper created by using different material ratio, different geometry, different boundary condition and parameters to quantize the effects of energy dissipation in form of structural, material damping as well as hysteresis. These 9 different types of dampers are shown in table 8 below

5.1 Different types of damper

Types	Configurations	Boundary conditions
TYPE 1	r=7mm, total length=86.29mm, gauge length=40,effective gauge length=21mm, bell shap	B.C 0
TYPE 2	t=16mm, r=150mm, r=165.5mm, r=185.5mm No Polyurethane, steel rods, U-shape	B.C 1
TYPE 3	t=16mm, r=150mm, r=165.5mm, r=185.5mm No Polyurethane, steel rods, U-shape	B.C 2
TYPE 4	t=20mm, t=25, r =150mm, No Polyurethane, steel rods, U-shape	B.C 1
TYPE 5	t=20mm, t=25, r =150mm, No Polyurethane, steel rods, U-shape	B.C 2
TYPE 6	Steel base=17mm, laminate=1mm, concentraining layer=3mm,U-shape	B.C 1
TYPE 7	Steel base=17mm, laminate=1mm, concentraining layer=3mm, U-shape	B.C 2
TYPE 8	Steel outer layer=10mm, steel inner layer=10mm ,Laminate thickness = 5mm/9mm, U-shape	B.C 2
TYPE 9	Steel outer layer=10mm, steel inner layer=10mm ,Laminate thickness = 11.5mm, U-shape	B.C 2

Table 9: Different types of damper for simulation

The results are for obtained for all the types in the form of frequency response function (FRF) and hysteresis loops in order to choose the best one having both the capability to avoid resonance as well as hysteretic dissipation. Numerical validation and mesh sensitivity

analysis is also performed. Dimensions of the dissipation plate in fig 35

Figure 35: Dimensions of U-Shaped steel plate

R is the mean radius of the damper while an extra parameter "r" is added which is the outer radius of the damper, "t" is the thickness and "H" is the height of plate

5.2 Numerical validation

As far as the validation of structural hysteresis is concerned, stress vs plastic strain curve is plotted taken from experimental results of the coupon test for the structural steel with ABAQUS results as shown in fig 36
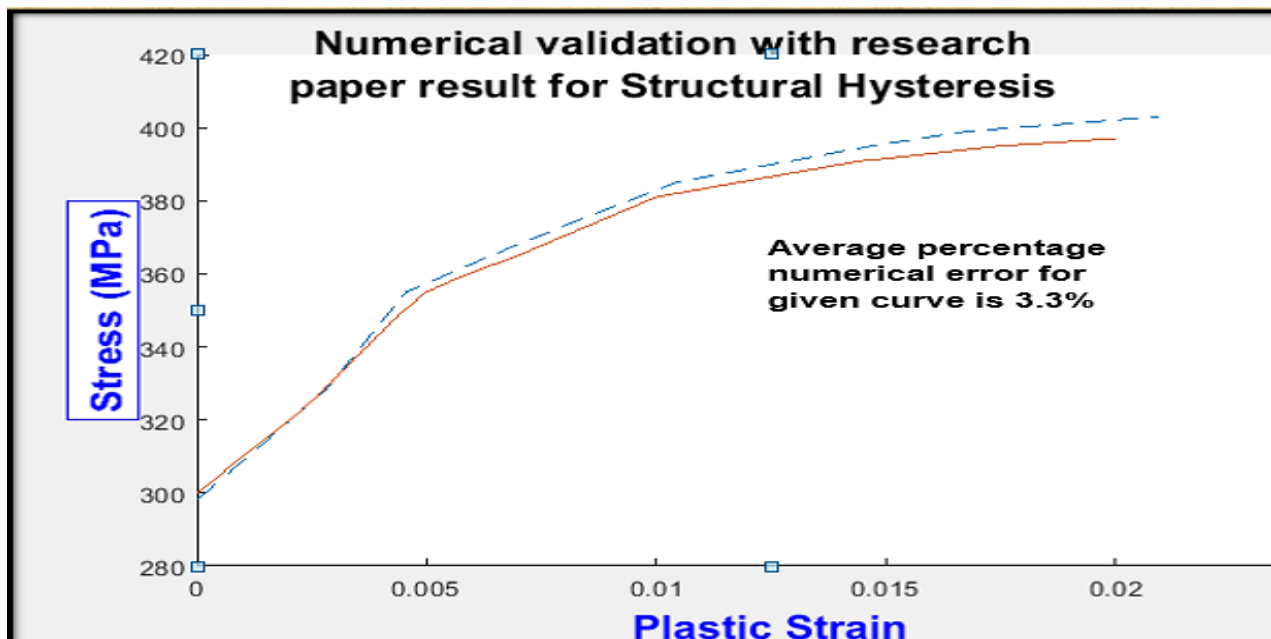
Figure 36: Numerical validation for structural hysteresis

While for the steady state analysis the analytical solution of the first mode shape of rectangular beam is calculated and compared with Abaqus results
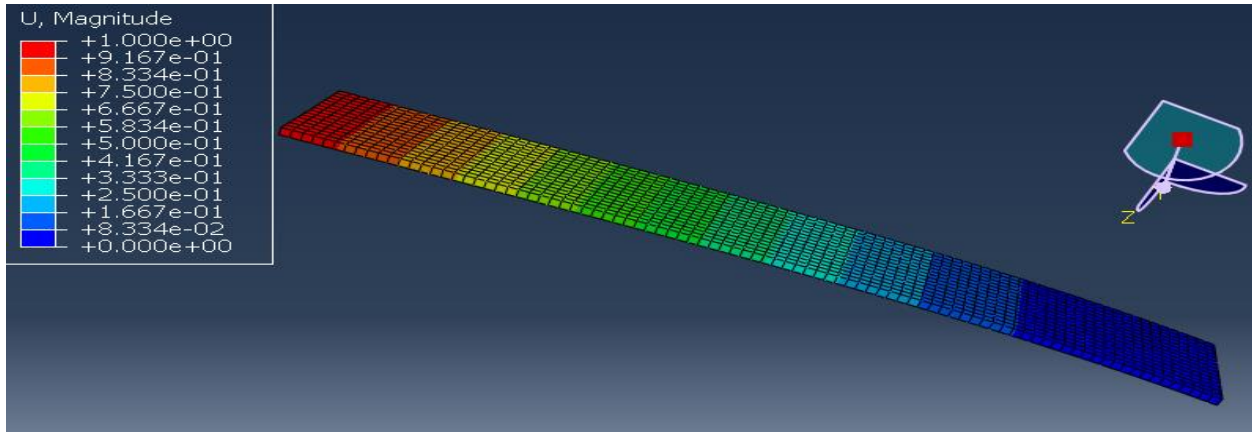
Figure 37: Numerical validation for first mode shape of rectangular beam

$$\boldsymbol{\omega} = \frac{(Bl)^2}{} \sqrt{\frac{EI}{\rho Al^2}}$$

Numerical error calculated is 2.3%

5.3 Mesh sensitivity analysis

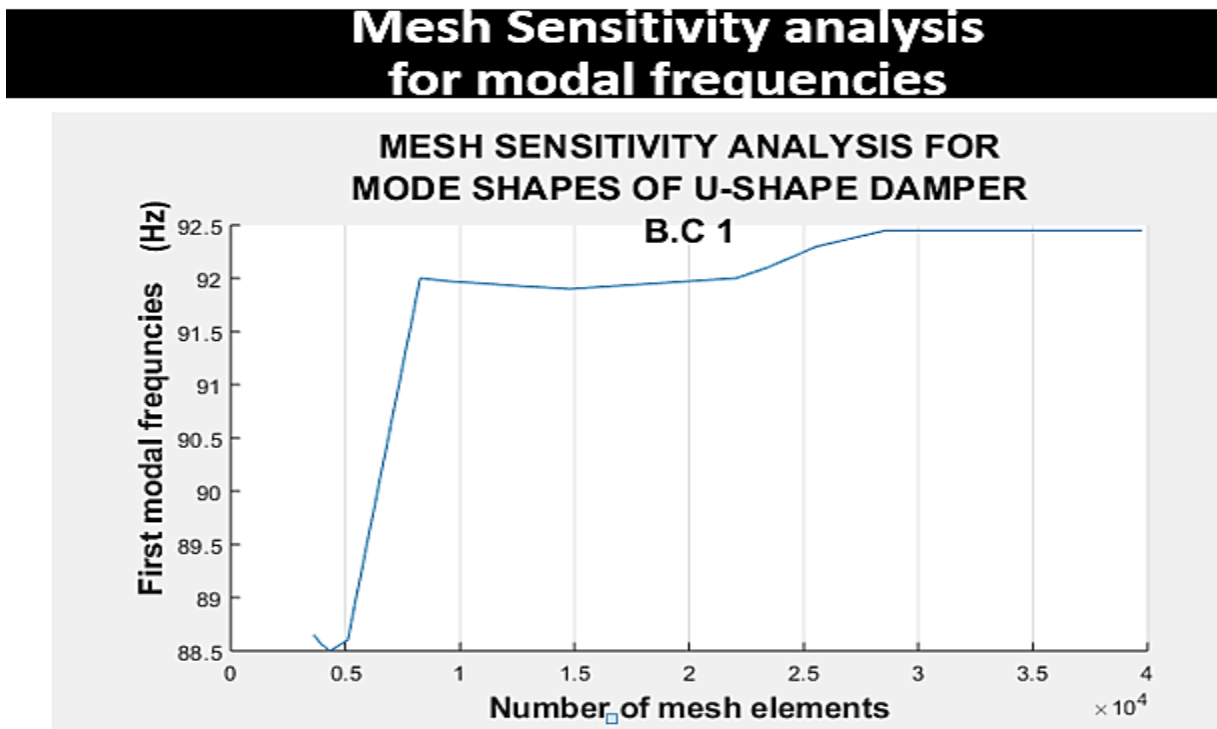The numerical solution results got stabilized and remains unchanged for finer mesh as below

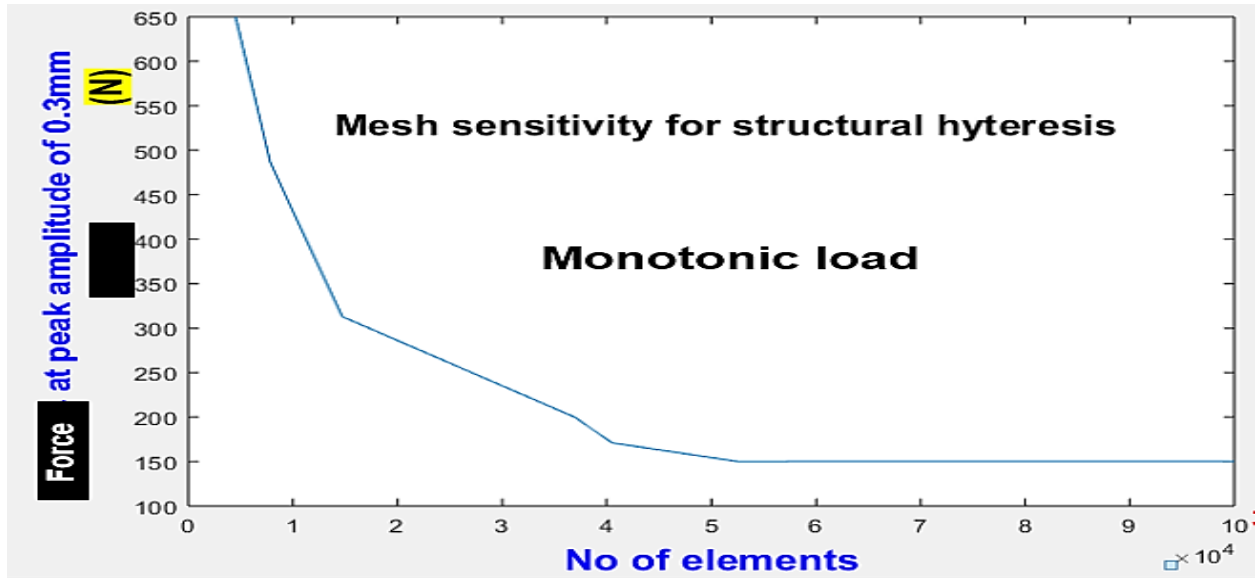*Figure 37.1: Mesh sensitivity analysis of dissipation plate for first mode*

Fig 37.2: Mesh sensitivity analysis for structural hysteresis monotonic load

5.4 Type 1 Cyclic response

Type 1 is the simple tensile test geometry with the parameters mentioned in table 9 and applied boundary condition with one end fixed and other is applied displacement in figure 38
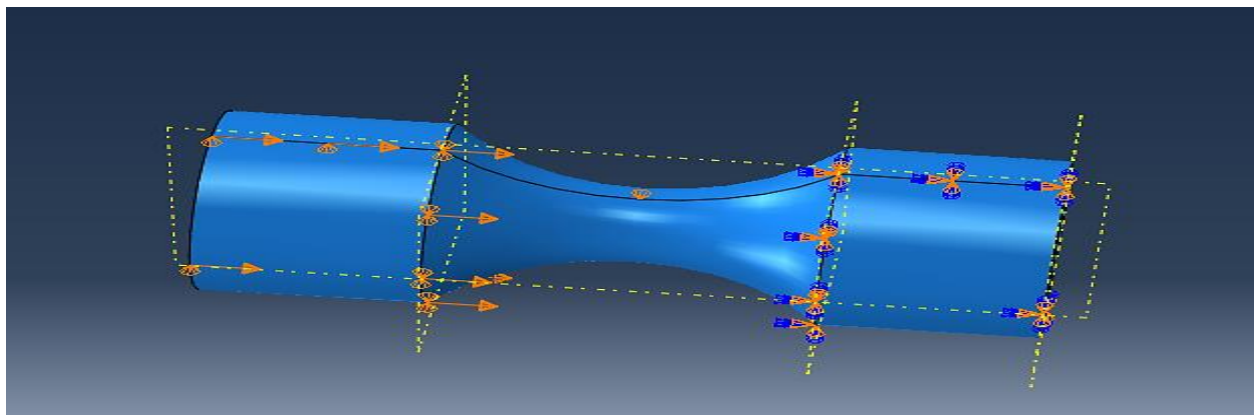

Figure 38: Type 1

The hysteresis loop is shown below with applied boundary condition of 1.5mm for outer loop and 0.7mm for inner loop in axial direction. These strain-controlled conditions are scaled by the tabular amplitude created in ABAQUS shown in fig 5.4.2, hysteresis loop in fig 39
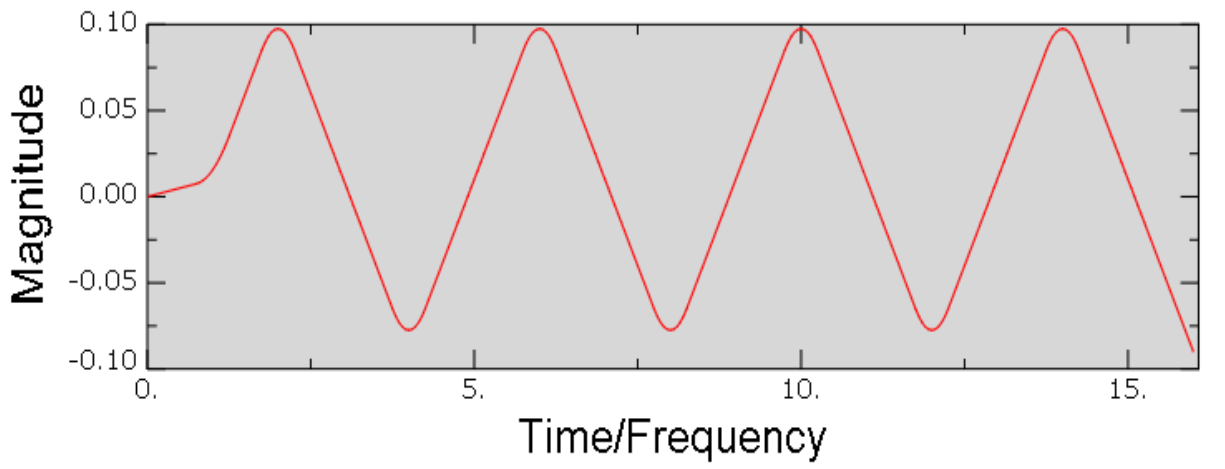
Figure 39: Scaling for strain control model

Outer loop disp =0.15mm
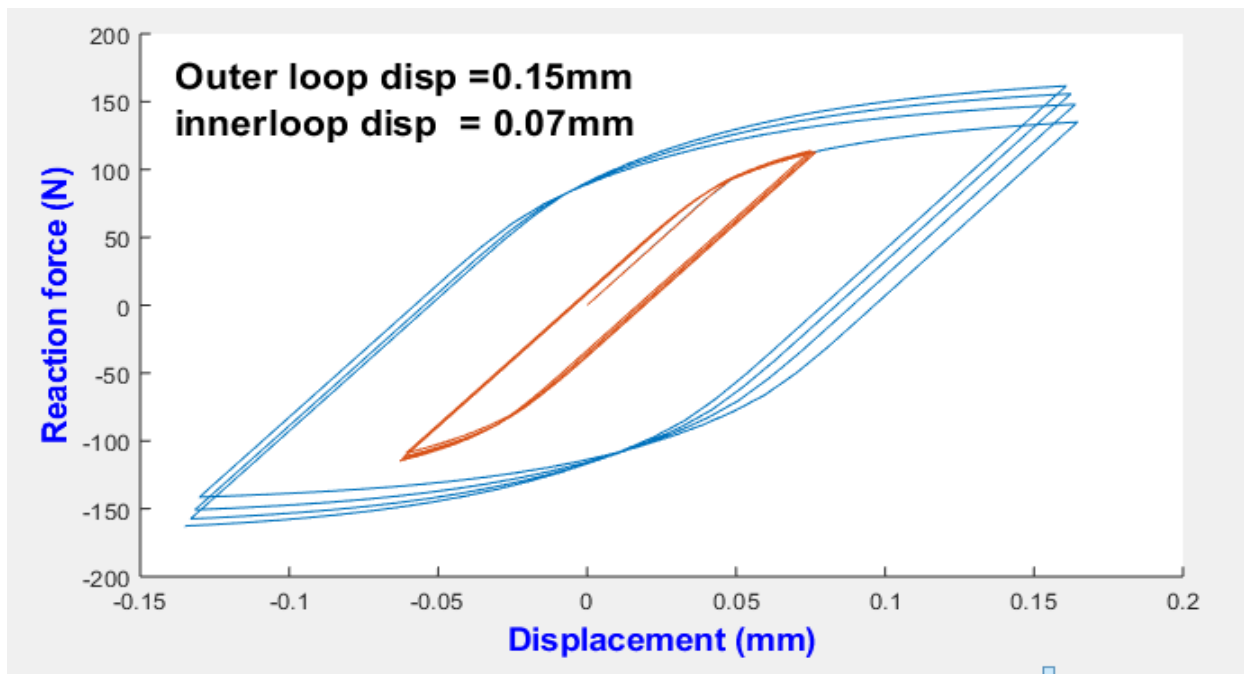innerloop disp = 0.07mm

Figure 40: Hysteresis loop for Type 1

These are the cyclic responses of the given shape regardless of fatigue life until the hysteresis loop got stabilized.

The result shows the clear effects of isotropic hardening as the loop got expanded and the kinematic hardening as the position of the loop is displaced so the Bauschinger effect is also clear. For the all coming types boundary conditions are specific for given type shown in fig
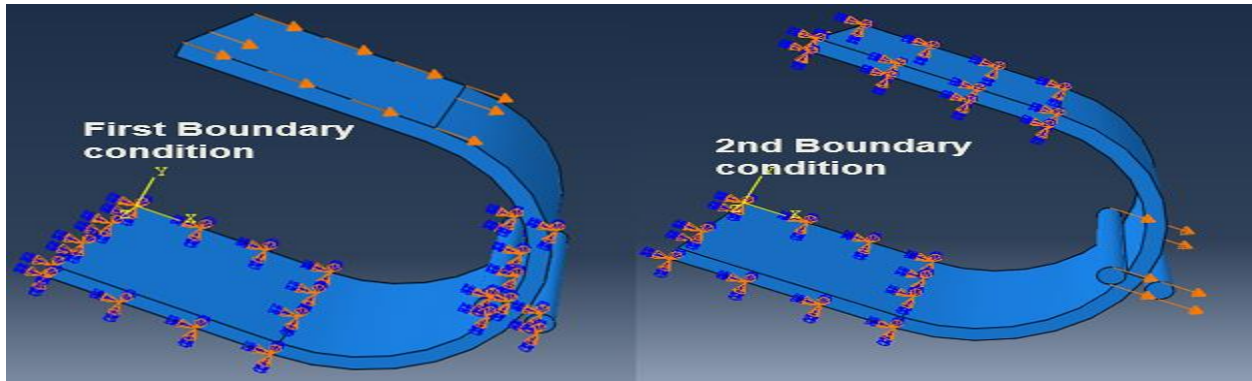
Figure 41: Slender steel rod for load transmission

5.5 Type 2

This type keeps the thickness of damper constant, varies the outer radius and uses boundary condition 1. The new steel rods have substituted the connection plates in a well manner in order to transmit load with modified boundary condition to enhance plastic deformation and sensitivity of damper. Rods of steel having radius 22mm and length 225mm. Steel rods are common in all the types from 1 to 9 and the geometry in all the types is in U-shape of steel except some lamination is used in coming types made of polyurethane.
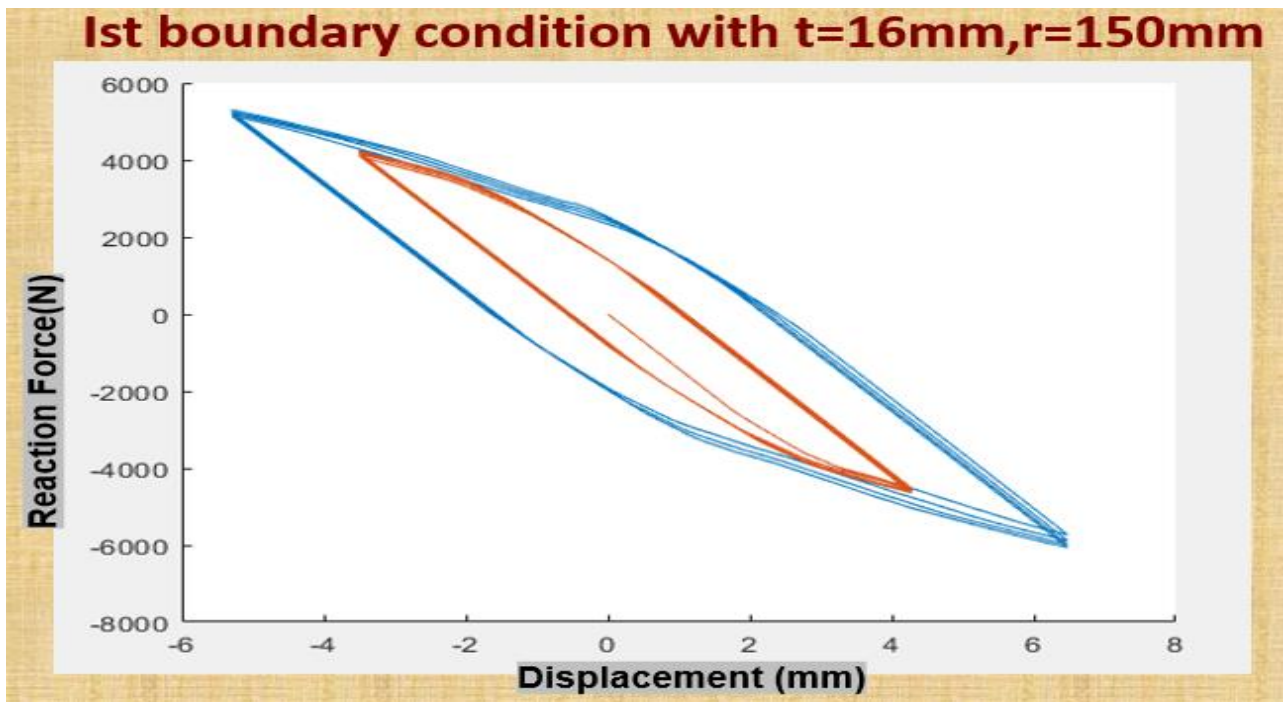

Figure 42: Hysteresis loop for type 2 at r=150mm
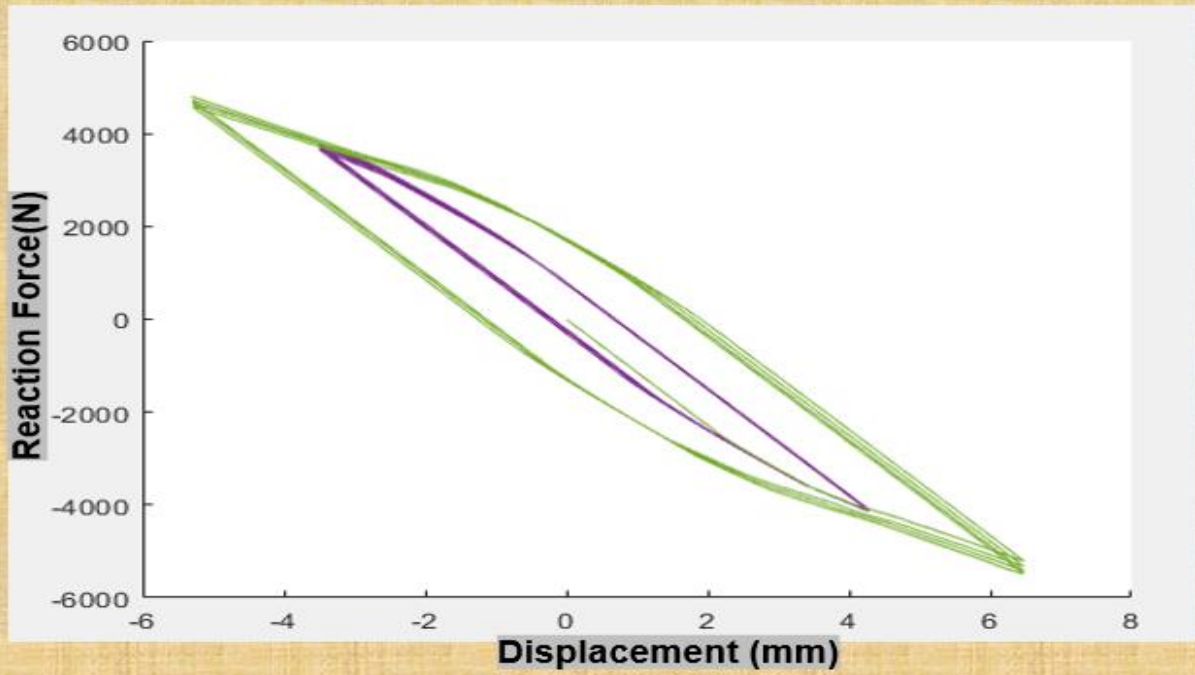
Figure 43: Hysteresis loop for type 2 at r=167.5mm

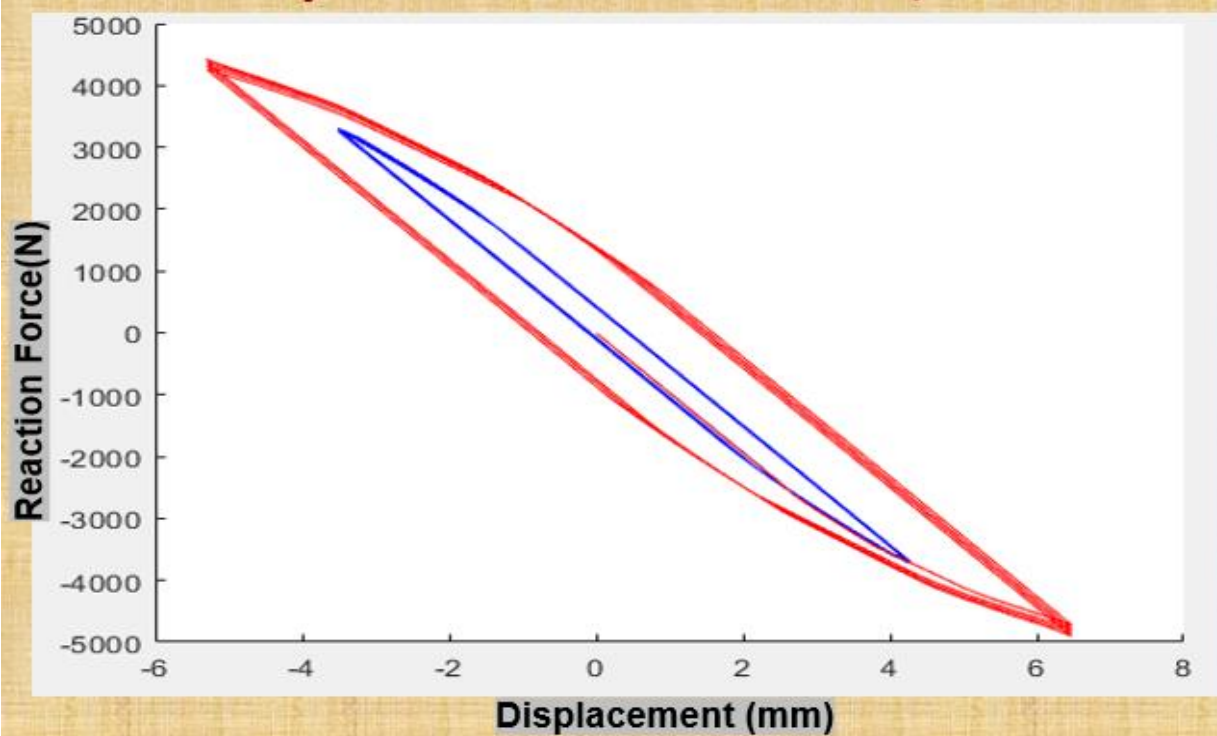*Figure 44: Hysteresis loop for type 2 at r=185.5mm*

5.6   Type 3
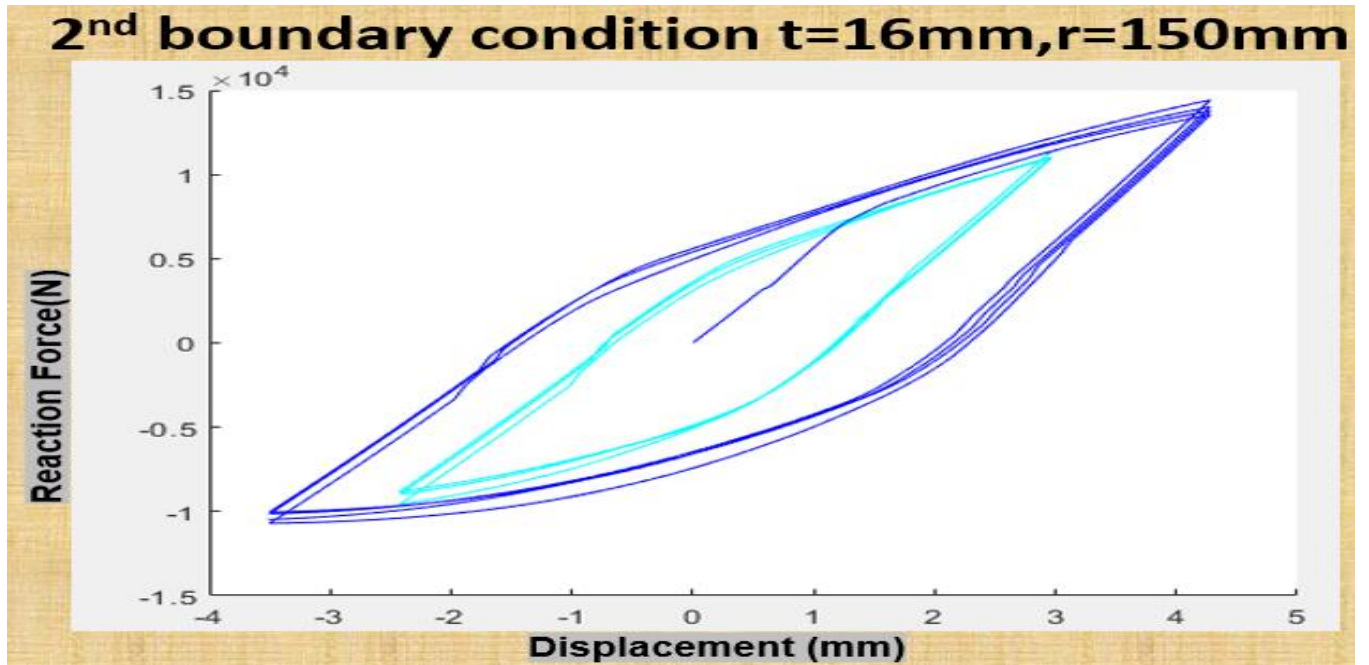
Figure 45: Hysteresis loop for type 3 at r=150mm
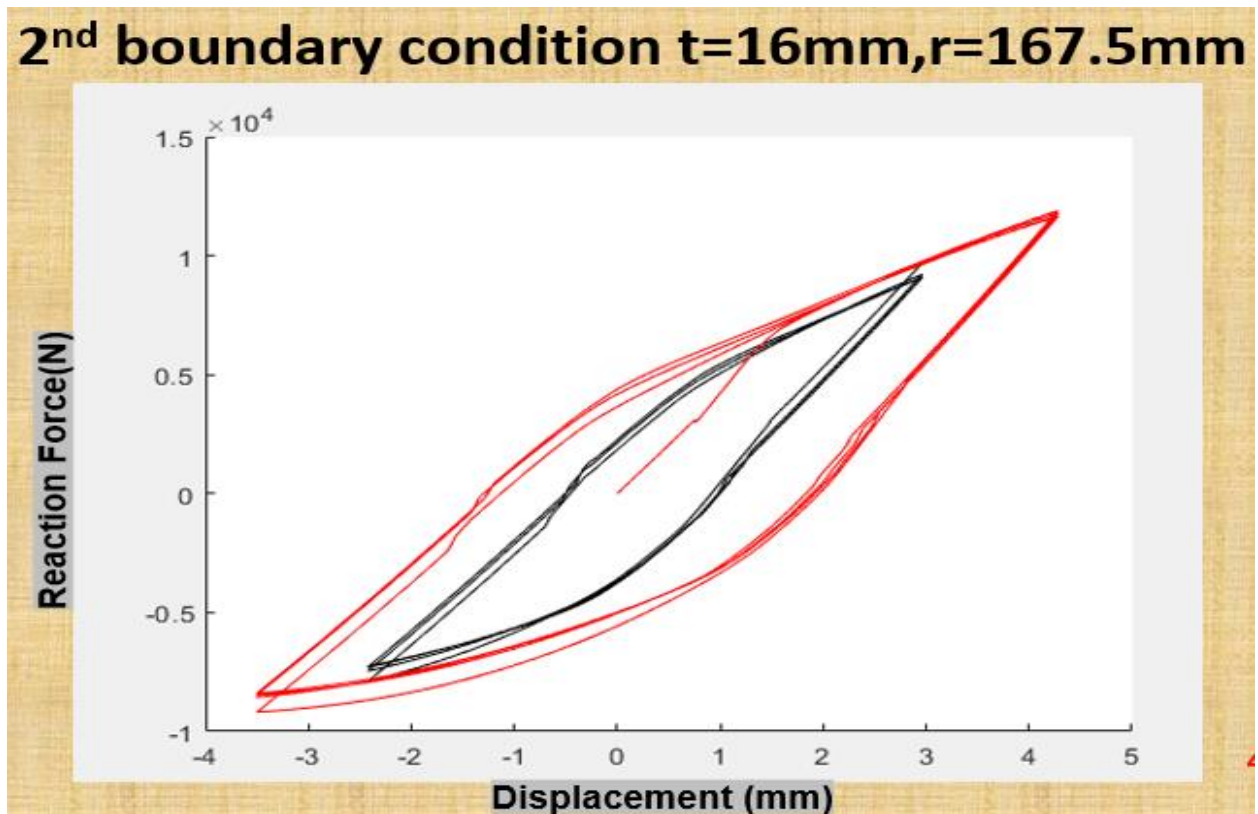
Figure 46: Hysteresis loop for type 3 at r=167.5mm
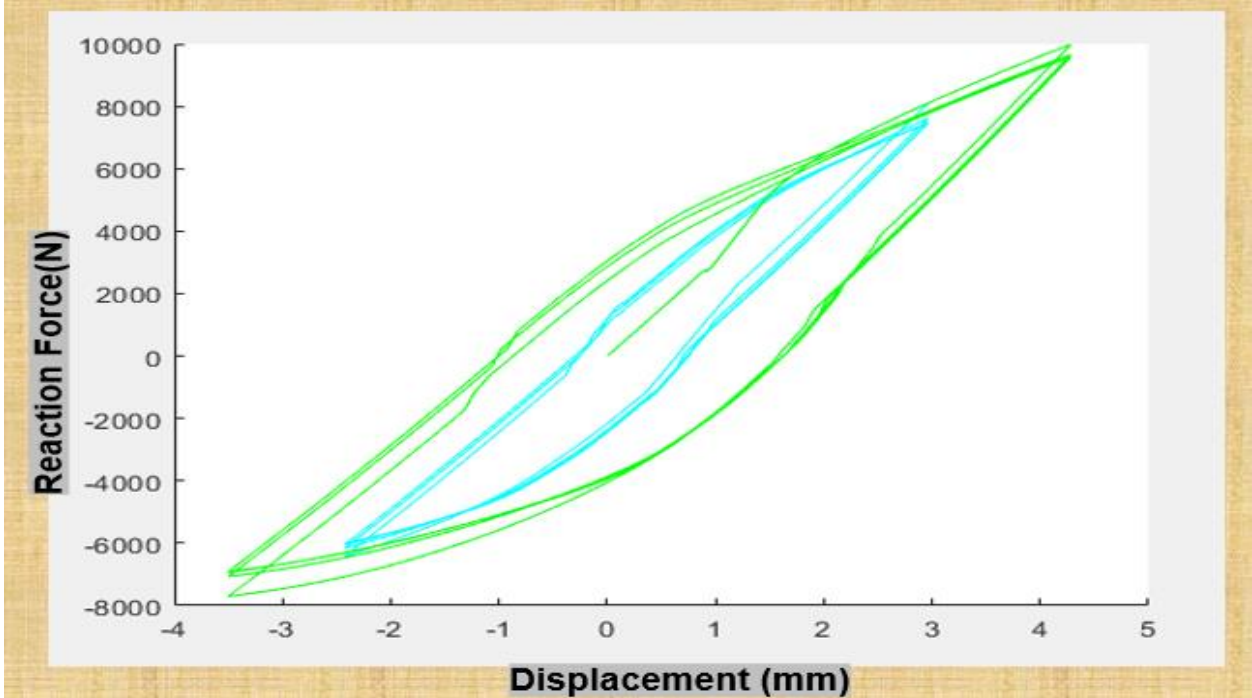
Figure 47: Hysteresis loop for type 3 at r=185.5mm

5.7 Type 4
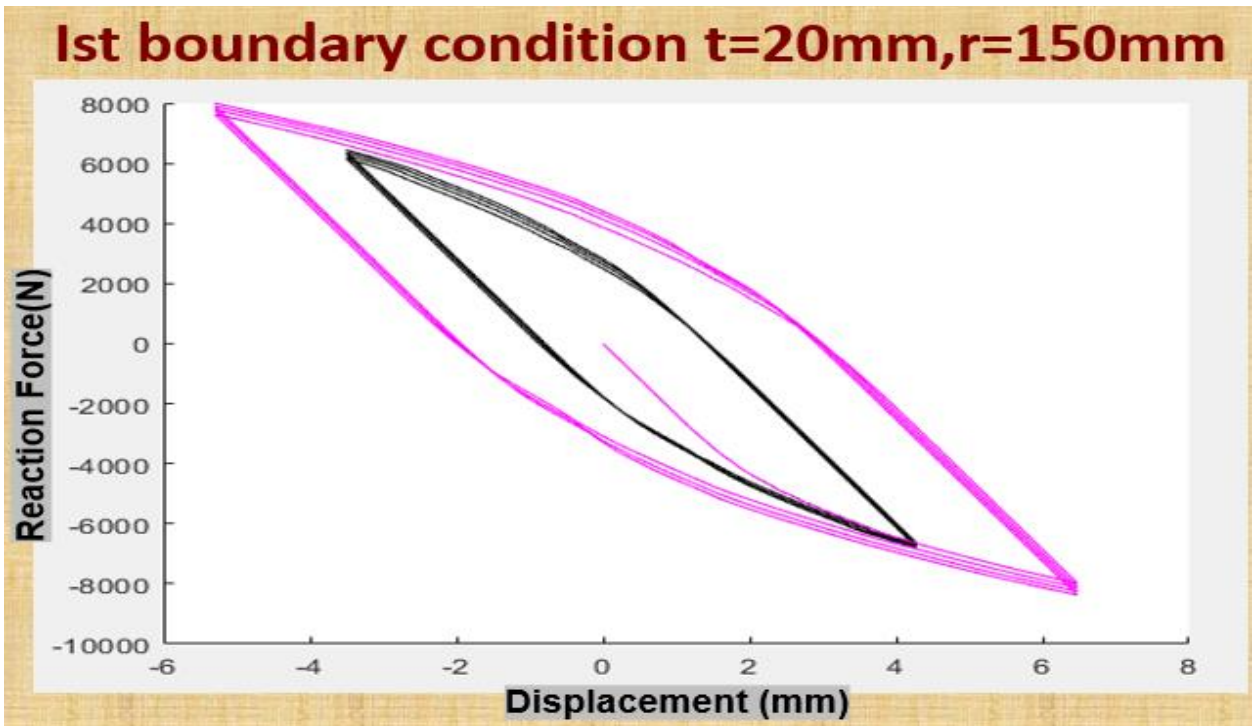
Figure 48:Hysteresis loop for type 4 at t=20mm
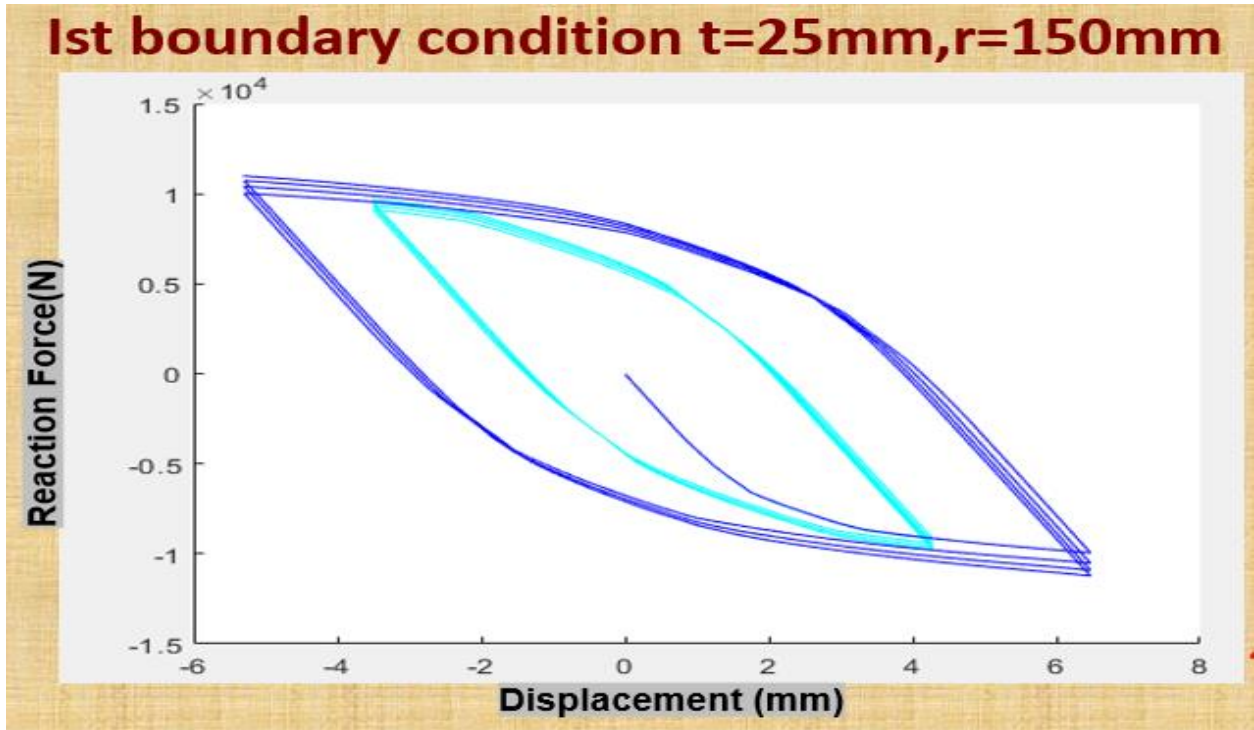
Figure 49: Hysteresis loop for type 4 at t=25mm

5.8 Type 5
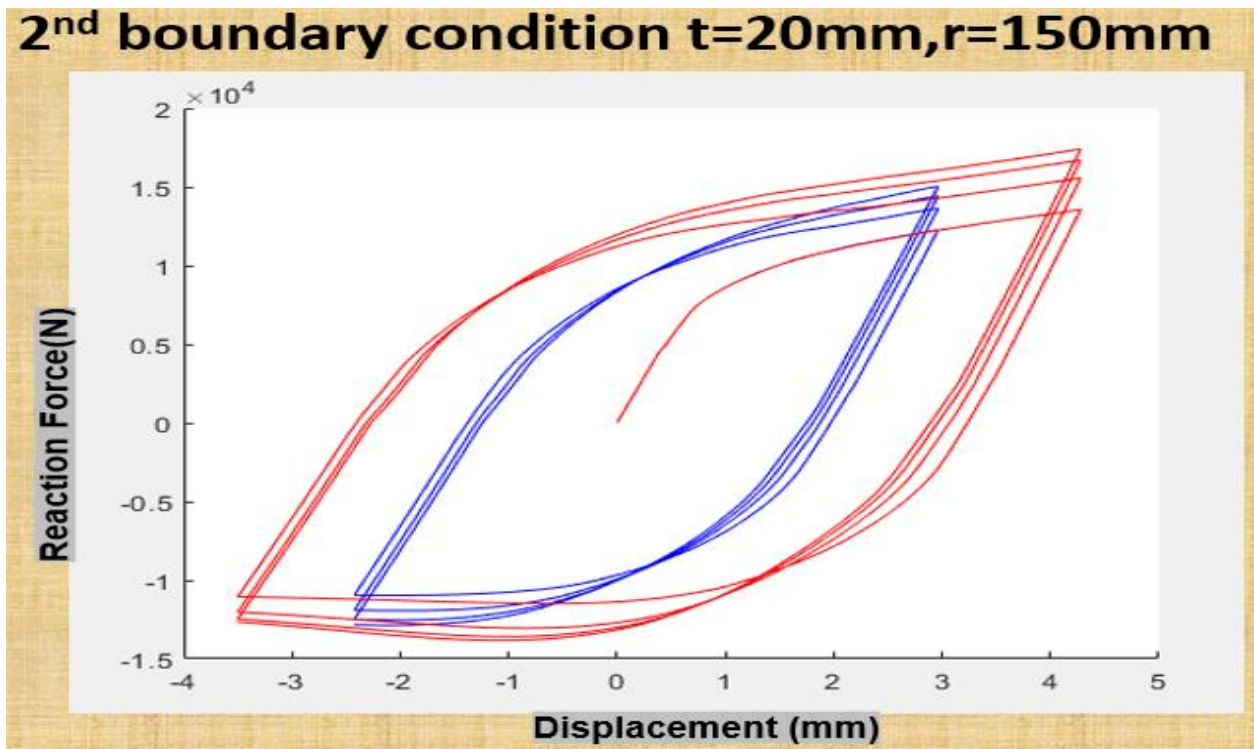
Figure 50: Hysteresis loop for type 5 at t=20mm
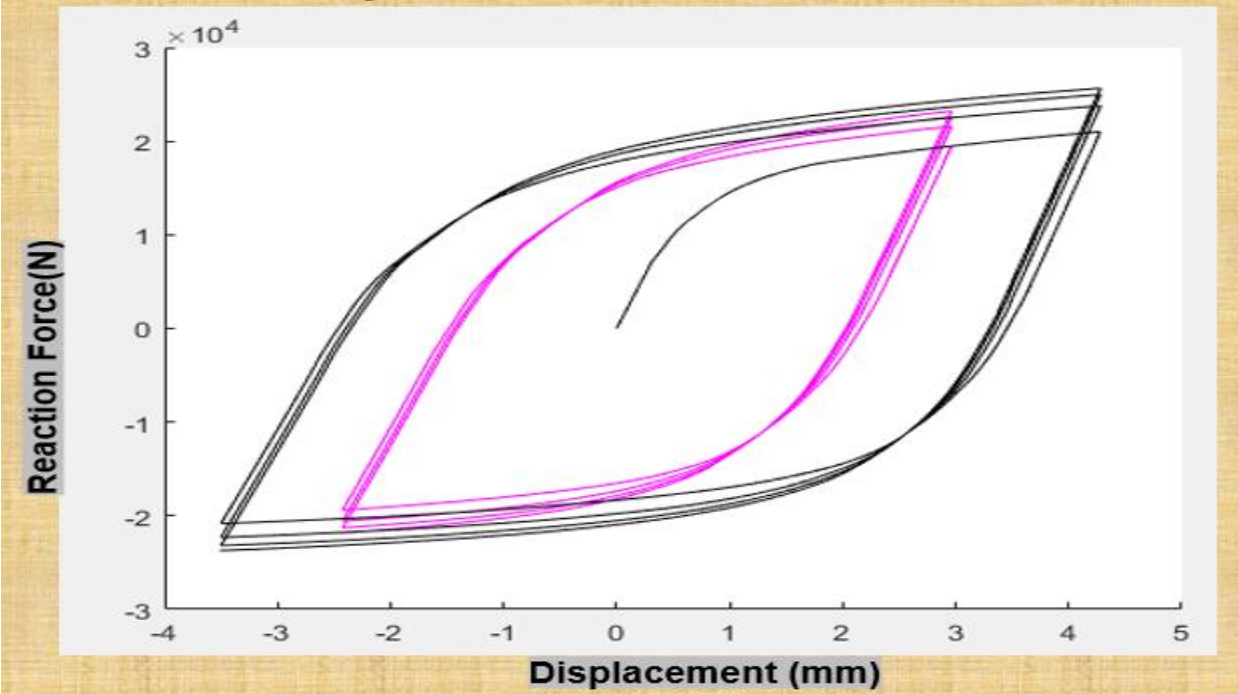
Figure 51: Hysteresis loop for type 5 at t=25mm

5.9 Mode Shape for first and second boundary condition for first mode. These shapes are same for all the types
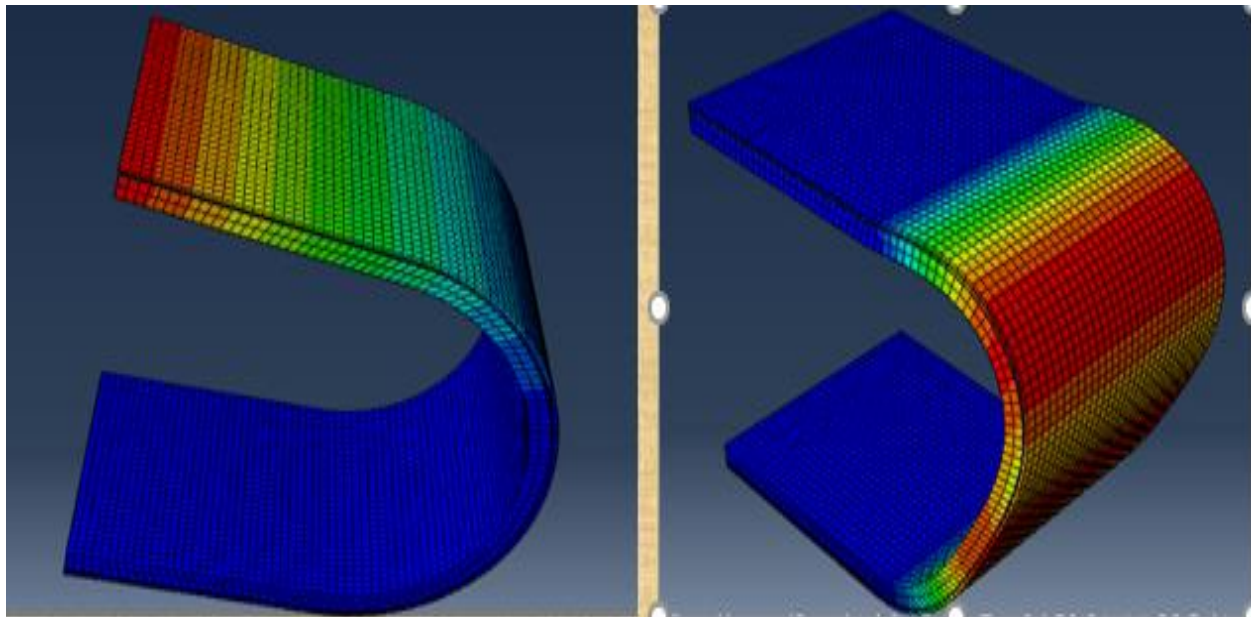
Figure 52: First mode shape for all types of dampers
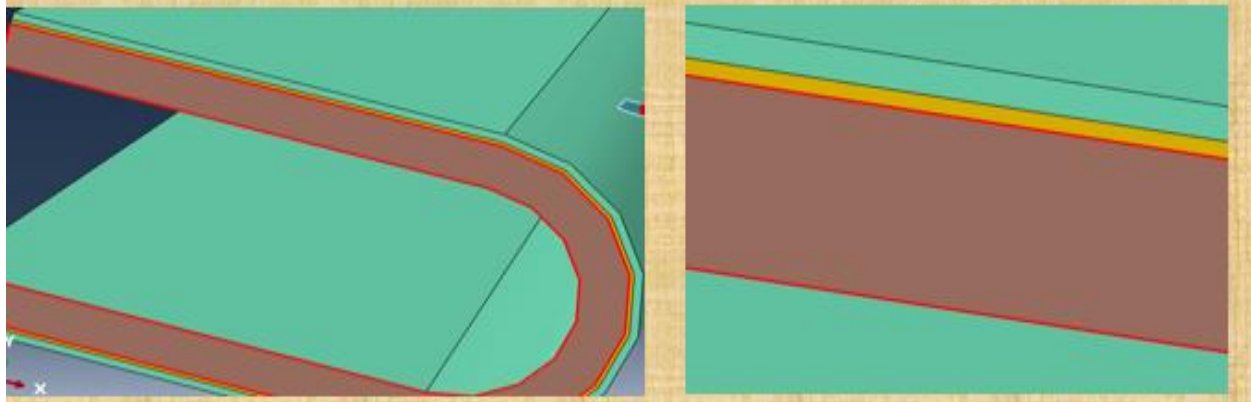
Figure 53: Steel base(red), polyurethane(yellow) and concentraining layer(green)

5.10 Modal Analysis FRF of type 6: compared with type pure steel damper having the parameters t=20mm, r =150mm
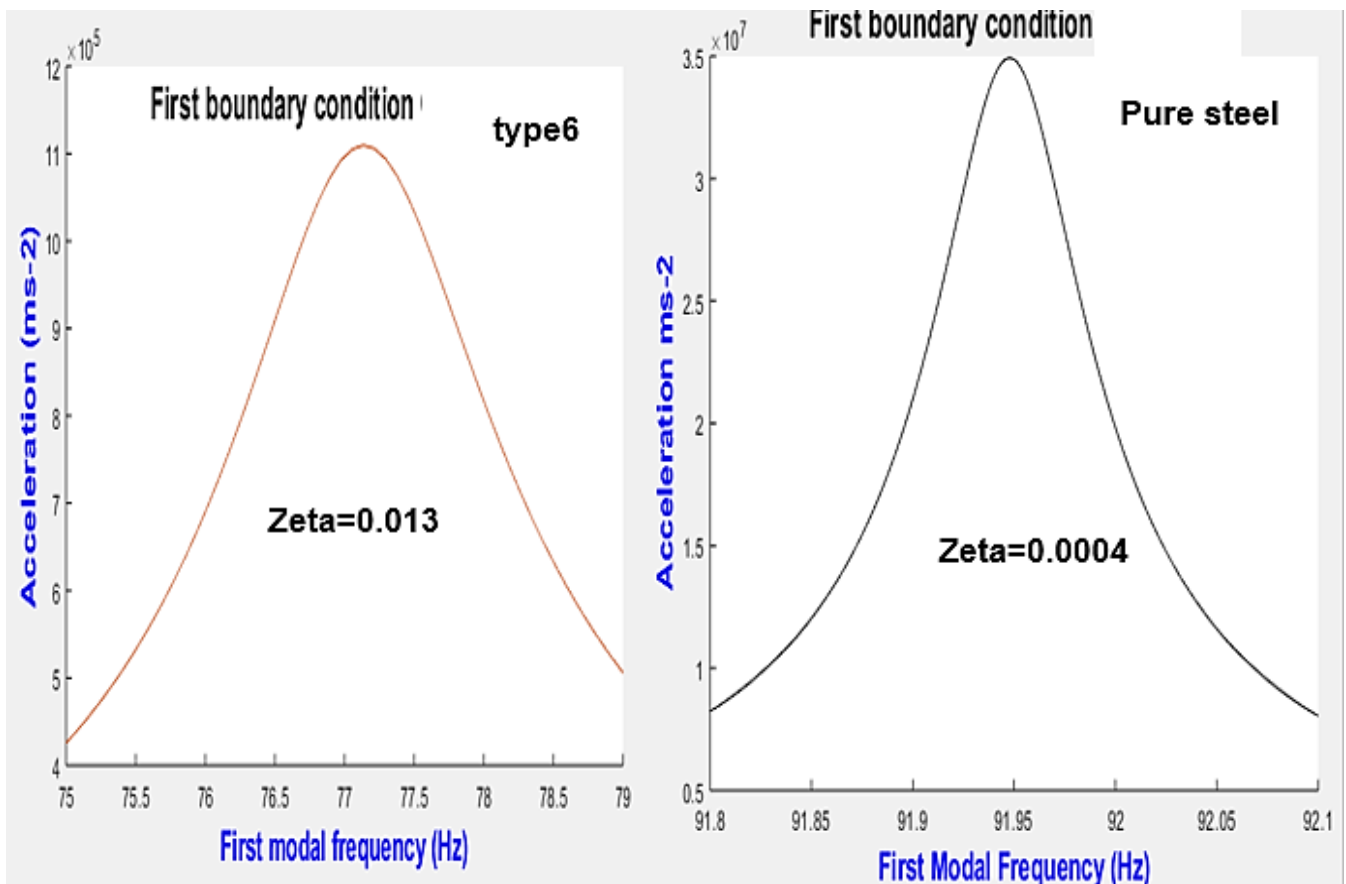
Figure 54: FRF first mode type6

5.11 Modal Analysis FRF of type 7, compared with type pure steel damper having the parameters t=20mm, r =150mm
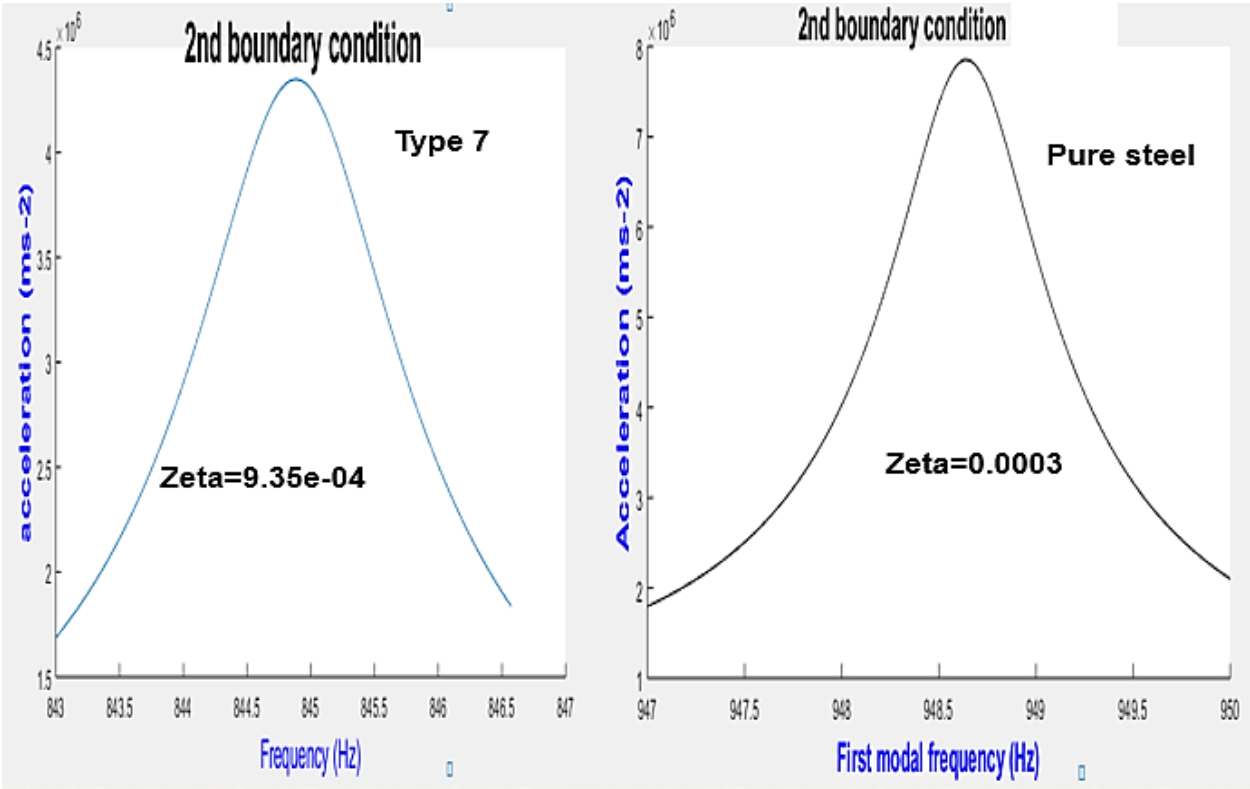
Figure 55: FRF first mode type 7

5.12 Type 8
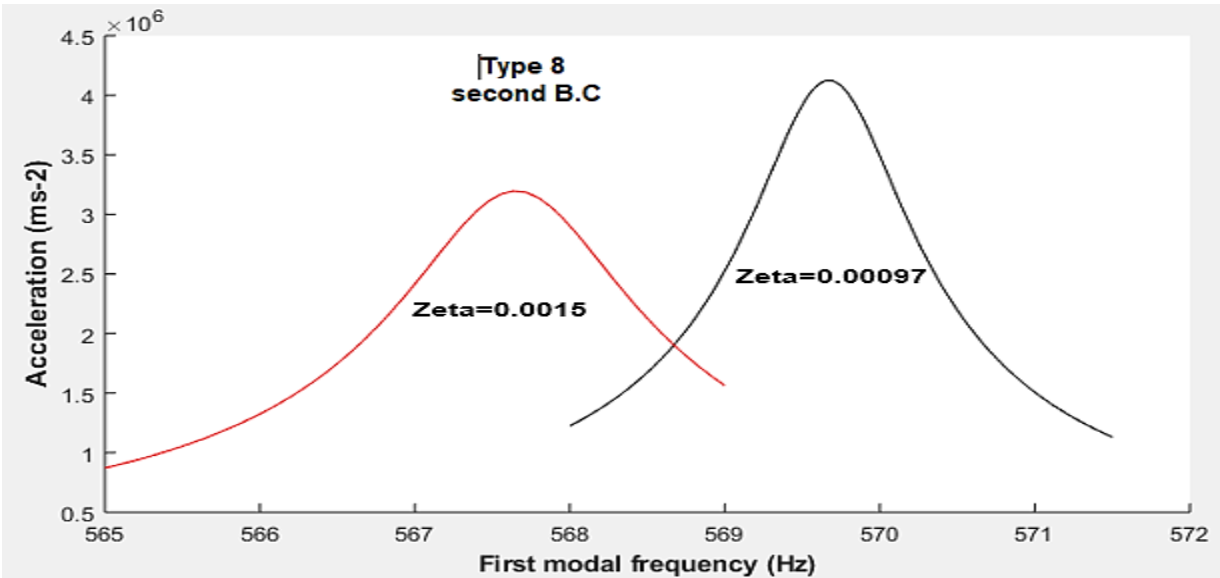
Figure 56: FRF first mode type 8

5.13   Type 9
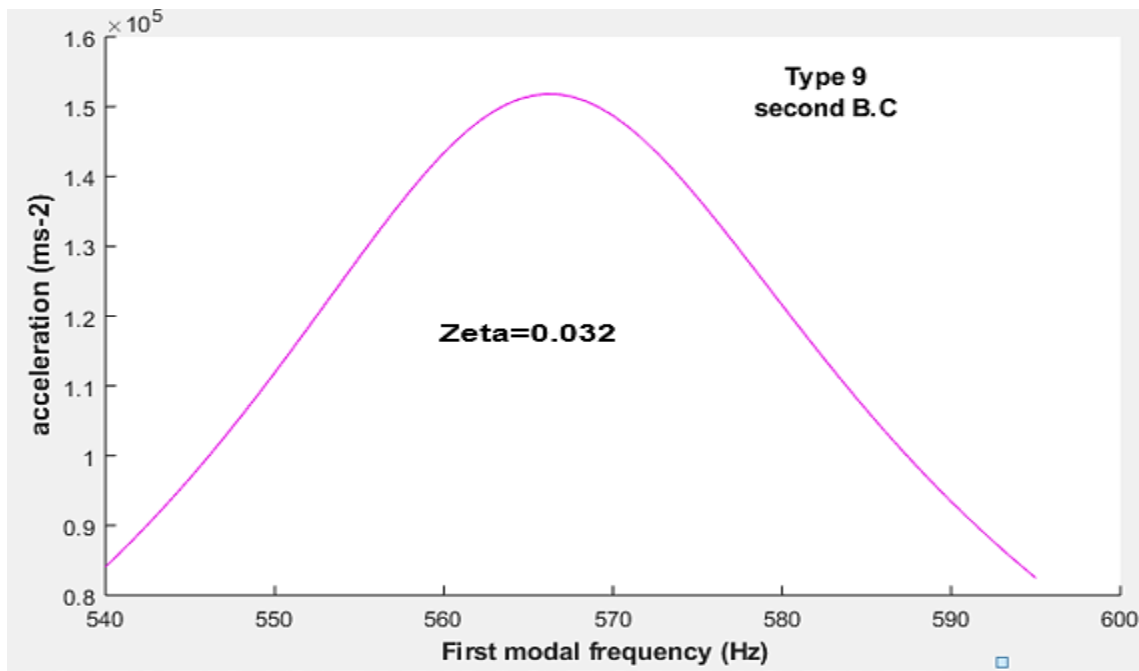
Figure 57: FRF first mode type 9

CHAPTER 6

Conclusions and Future scope of work

A thorough analysis of the current literature was conducted to define the purpose and breadth of the current studies. The literature review points out novelty of the work for both structural hysteresis and viscoelastic damping by varying material ratio in order to prevent seismic fragility and capable of interfering seismic drift for different intensities It is single geometry which is type 9 is the best among the 8 behaves as multipurpose and need of the isolation systems are reduced to suitable extent. Due to its passive damping ability it is cost effective needs no power supply, sensors with complete feedback control mechanisms and hence reliable due to little exposure towards damage. Easy to manufacture and the shape is adoptable towards installation.

6.1   CONCLUSIONS

1. Hysteresis energy of boundary condition 2>boundary 1>Previous boundary condition

2. Introduction of slender steel rods has significant effect on yielding and plastic deformation rather than connection plate assembly with large stiffness

3. By increasing the radius of damper will decrease the hysteresis energy while increasing thickness of damper will increase hysteresis energy for the constant displacement scaled by given amplitude

4. Modified system is displacement sensitive and able to damp light/heavy vehicular and from low to high seismic intensities with combined effect of structural and material damping

5. The ideal type for damper is selected as type 9 due to its high first modal frequency as compared to vehicle-bridge resonant mode

6. The value of damping ratio for type 9>type6>type8>type7

7. Where there is second boundary condition the thickness of polyurethane laminate required is 11.5 times more than the boundary condition 1 in order to obtain the value of zeta greater but closer to boundary condition 1

8. For the same laminate thickness the value of zeta for boundary condition 1 is 14 times greater than boundary condition 2 for the same thickness of 1mm polyurethane laminate

9. Type 9 achieves good damping but on the expense of thickness which is further altered by placing laminate in the free region

6.2   SCOPE FOR FUTURE RESEARCH

- ➢ Optimization tasks between different parameters can be performed like hysteresis energy to volume/mass, fatigue life to geometry, thickness, radius of damper etc
- ➢ Fatigue life, corrosion, manufacturing advancements leads to design.
- ➢ Dynamic machines and static machine vibration analysis of type 9 can be performed because of huge research gap
- ➢ Fracture analysis and crack propagation analysis can be performed
- ➢ Generating effective regions to install damper rather than pier and girder, improving boundary conditions
- ➢ By parametrizing the need for isolation systems will simply lead to substitute the system by type 9.
- ➢ Combination of different types can be performed for effective damping

REFERENCES

1-Lee, E., Stoughton, T. and Yoon, J. (2018). Kinematic hardening model considering directional hardening response. International Journal of Plasticity, 110, pp.145-165.

2-Li, Z., Shu, G. and Huang, Z. (2019). Development and cyclic testing of an innovative shear-bending combined metallic damper. Journal of Constructional Steel Research, 158, pp.28-40.

3- Jarrah, M., Khezrzadeh, H., Mofid, M. and Jafari, K. (2019). Experimental and numerical evaluation of piston metallic damper (PMD). Journal of Constructional Steel Research, 154, pp.99-109.

4-Xu, X., Li, Z., Liu, W., Feng, D. and Li, X. (2019). Investigation of the wind-resistant performance of seismic viscous dampers on a cable-stayed bridge.

5-Deng, K., Pan, P. and Wang, C. (2019). Development of crawler steel damper for bridges.

6-Wijaya, H., Rajeev, P., Gad, E. and Amirsardari, A. (2019). Effect of hysteretic steel damper uncertainty on seismic performance of steel buildings. Journal of Constructional Steel Research, 157, pp.46-58.

7-Yang, Y., Lin, C. and Yau, J. (2004). Extracting bridge frequencies from the dynamic response of a passing vehicle. Journal of Sound and Vibration, 272(3-5), pp.471-493.

8-Narendra, P., Prasad, K., Krishna, E., Kumar, V. and Singh, K. (2019). Low-Cycle-Fatigue (LCF) behavior and cyclic plasticity modeling of E250A mild steel. *Structures*, 20, pp.594-606.

9-Okorokov, V., Gorash, Y., Mackenzie, D. and van Rijswick, R. (2019). New formulation of nonlinear kinematic hardening model, Part II: Cyclic hardening/softening and ratcheting. *International Journal of Plasticity*.

10-Han, S., Shi, D., Yang, X., Huang, J. and Sun, Y. (2018). A hypothetical dislocation well model for kinematic hardening in cyclic plasticity. *International Journal of Plasticity*, 110, pp.220-247.

11-Badreddine, H., Saanouni, K., Labergère, C. and Duval, J. (2018). Effect of the kinematic hardening on the plastic anisotropy parameters for metallic sheets. *Comptes Rendus Mécanique*, 346(8), pp.678-700.

12-Chang, Y., Noormohamed, A. and Mercan, O. (2018). Analytical and experimental investigations of Modified Tuned Liquid Dampers (MTLDs). *Journal of Sound and Vibration*, 428, pp.179-194.

13-Garrido, H., Curadelli, O. and Ambrosini, D. (2013). Improvement of tuned mass damper by using rotational inertia through tuned viscous mass damper. *Engineering Structures*, 56, pp.2149-2153.

14-Christie, M., Sun, S., Deng, L., Ning, D., Du, H., Zhang, S. and Li, W. (2019). A variable resonance magnetorheological-fluid-based pendulum tuned mass damper for seismic vibration suppression. *Mechanical Systems and Signal Processing*, 116, pp.530-544.

15-Nesládek, M. and Španiel, M. (2017). An Abaqus plugin for fatigue predictions. *Advances in Engineering Software*, 103, pp.1-11.

16-Lotfi Mahyari, S., Tajmir Riahi, H. and Hashemi, M. (2019). Investigating the analytical and experimental performance of a pure torsional yielding damper. *Journal of Constructional Steel Research*, 161, pp.385-399.

17-Genikomsou, A. and Polak, M. (2015). Finite element analysis of punching shear of concrete slabs using damaged plasticity model in ABAQUS. *Engineering Structures*, 98, pp.38-48.

18-Zhang, R., Wang, C., Pan, C., Shen, H., Ge, Q. and Zhang, L. (2018). Simplified design of elastoplastic structures with metallic yielding dampers based on the concept of uniform damping ratio. *Engineering Structures*, 176, pp.734-745.

19-Dong, X., BiFeng, S., WenQing, Y. and Peng, F. (2015). Structural Damping Effect on Deformation of Flexible Flapping Wing. *Procedia Engineering*, 99, pp.1365-1371.

21- Arora, V. (2015). Direct structural damping identification method using complex FRFs. *Journal of Sound and Vibration*, 339, pp.304-323.

22-Mevada, H. and Patel, D. (2016). Experimental Determination of Structural Damping of Different Materials. *Procedia Engineering*, 144, pp.110-115.

23-Foti, F., Martinelli, L. and Perotti, F. (2017). A parametric study on the structural damping of suspended cables. *Procedia Engineering*, 199, pp.140-145.

24-Qiu, C., Zhang, Y., Qu, B., Dai, C., Hou, H. and Li, H. (2019). Cyclic testing of seismic dampers consisting of multiple energy absorbing steel plate clusters. *Engineering Structures*, 183, pp.255-264.

26-Qu, B., Dai, C., Qiu, J., Hou, H., & Qiu, C. (2019). Testing of seismic dampers with replaceable U-shaped steel plates. *Engineering Structures*, *179*, 625-639.

27-Xu, L. Y., Nie, X., & Fan, J. S. (2016). Cyclic behaviour of low-yield-point steel shear panel dampers. *Engineering Structures*, *126*, 391-404.

28-Ranaei, O., & Aghakouchak, A. A. (2019). A new hybrid energy dissipation system with viscoelastic and flexural yielding strips dampers for multi-level vibration control. *Archives of Civil and Mechanical Engineering*, *19*(2), 584-597.

29-Khatibinia, M., Jalali, M., & Gharehbaghi, S. (2019). Shape optimization of U-shaped steel dampers subjected to cyclic loading using an efficient hybrid approach. *Engineering Structures*, 108874.

30-Chen, Y., Chen, C., Jiang, H., Liu, T., & Wan, Z. (2019). Study of an innovative graded yield metal damper. *Journal of Constructional Steel Research*, *160*, 240-254.

31-Liu, Y., Guo, Z., Liu, X., Chicchi, R., & Shahrooz, B. (2019). An innovative resilient rocking column with replaceable steel slit dampers: Experimental program on seismic performance. *Engineering Structures*, *183*, 830-840.

32-Zhou, L., Wang, X., & Ye, A. (2019). Low cycle fatigue performance investigation on Transverse Steel Dampers for bridges under ground motion sequences using shake-table tests. *Engineering Structures*, *196*, 109328.

33-Shen, H., Zhang, R., Weng, D., Gao, C., Luo, H., & Pan, C. (2017). Simple design method of structure with metallic yielding dampers based on elastic–plastic response reduction curve. *Engineering Structures*, *150*, 98-114.

34-Farzampour, A., & Eatherton, M. R. (2019). Yielding and lateral torsional buckling limit states for butterfly-shaped shear links. *Engineering Structures*, *180*, 442-451.

35-Yano, D., Ishikawa, S., Tanaka, K., & Kijimoto, S. (2019). Vibration analysis of viscoelastic damping material attached to a cylindrical pipe by added mass and added damping. *Journal of Sound and Vibration*, *454*, 14-31.

36-Zhong, Y., Tu, J., Yu, Y., Xu, J., & Tan, D. (2017). Temperature compensation in viscoelastic damper using magnetorheological effect. *Journal of Sound and Vibration*, *398*, 39-51.

37-Bhaskar, N. M., Suresh, P. M., Babu, S., & Chandru, B. T. (2018). Numerical and Experimental Modal Analysis of Car Roof Incorporating Viscoelastic Damper. *Materials Today: Proceedings*, *5*(10), 22254-22261.

38-Burlon, A., Failla, G., & Arena, F. (2016). Exact frequency response analysis of axially loaded beams with viscoelastic dampers. *International Journal of Mechanical Sciences*, *115*, 370-384.

39-Yamazaki, S., Usami, T., & Nonaka, T. (2016). Developing a new hysteretic type seismic damper (BRRP) for steel bridges. *Engineering Structures*, *124*, 286-301.

40-Aydin, E., Öztürk, B., & Dutkiewicz, M. (2019). Analysis of efficiency of passive dampers in multistorey buildings. *Journal of Sound and Vibration*, *439*, 17-28.

41-Saige, D., Engelhardt, J., & Katz, S. (2017). Application of eddy current damper technology for passive tuned mass damper systems within footbridges. *Procedia engineering*, *199*, 1804-1809.

42-Hemmati, A., Oterkus, E., & Barltrop, N. (2019). Fragility reduction of offshore wind turbines using tuned liquid column dampers. *Soil Dynamics and Earthquake Engineering*, *125*, 105705.

43-Aghlara, R., Tahir, M. M., & Adnan, A. B. (2018). Experimental study of Pipe-Fuse Damper for passive energy dissipation in structures. *Journal of Constructional Steel Research*, *148*, 351-360.

44-Latour, M., Piluso, V., & Rizzano, G. (2018). Experimental analysis of beam-to-column joints equipped with sprayed aluminium friction dampers. *Journal of Constructional Steel Research*, *146*, 33-48.

45-Milani, A. S., & Dicleli, M. (2017). Low-cycle fatigue performance of solid cylindrical steel components subjected to torsion at very large strains. *Journal of Constructional Steel Research*, *129*, 12-27.

46-Taiyari, F., Mazzolani, F. M., & Bagheri, S. (2019). A proposal for energy dissipative braces with U-shaped steel strips. *Journal of Constructional Steel Research*, *154*, 110-122.

47- Casciati, F., Cimellaro, G. P., & Domaneschi, M. (2008). Seismic reliability of a cable-stayed bridge retrofitted with hysteretic devices. *Computers & Structures*, *86*(17-18), 1769-1781.

CERTIFICATE OF COMPLETENESS

It is hereby certified that the dissertation submitted by **NS Muhammad Saad Ali** Reg No.

00000204464, **Parametric study of Seismic-Vehicular damping using Structural hysteresis**

and viscoelastic material has been checked/reviewed and its contents are complete in all respects.

Supervisor's Name: **Dr. Hasan Aftab Saeed**   Signature: _____

Date: _____